AFWL-TR-76-115

AFWL-TR-
76-115

A 15 KILOWATT CW CO_2 COAXIAL ELECTRIC DISCHARGE LASER

August 1976

Final Report

Approved for public release; distribution unlimited.

AIR FORCE WEAPONS LABORATORY
Air Force Systems Command
Kirtland Air Force Base, NM 87117

This final report was prepared by the Air Focre Weapons Laboratory, Kirtland Air Force Base, New Mexico under Job Order 317J1097. Randolph L. Carlson (ALC) was the Laboratory Project Officer-in-Charge.

When US Government drawings, specifications, or other data are used for any purpose other than a definitely related Government procurement operation, the Government thereby incurs no responsibility nor any obligation whatsoever, and the fact that the Government may have formulated, furnished, or in any way supplied the said drawings, specifications, or other data is not to be regarded by implication or otherwise as in any manner licensing the holder or any other person or corporation or conveying any rights or permission to manufacture use, or sell any patented invention that may in any way be related thereto.

This report has been reviewed by the Information Office (OI) and is releasable to the National Technical Information Service (NTIS). At NTIS, it will be available to the general public, including foreign nations.

This technical report has been reviewed and is approved for publication.

Randolph L. Carlson
RANDOLPH L. CARLSON
Project Officer

FOR THE COMMANDER

Hector Rede
HECTOR REDE
Major, USAF
Chief, Effects and Vulnerability Branch

Louis H. Bernasconi
LOUIS H. BERNASCONI
Colonel, USAF
Chief, LEAPS Division

DO NOT RETURN THIS COPY. RETAIN OR DESTROY.

UNCLASSIFIED

SECURITY CLASSIFICATION OF THIS PAGE (When Data Entered)

REPORT DOCUMENTATION PAGE

READ INSTRUCTIONS BEFORE COMPLETING FORM

1. REPORT NUMBER: AFWL-TR-76-115
2. GOVT ACCESSION NO.
3. RECIPIENT'S CATALOG NUMBER
4. TITLE (and Subtitle): A 15 KILOWATT CW CO_2 COAXIAL ELECTRIC DISCHARGE LASER.
5. TYPE OF REPORT & PERIOD COVERED: Final Report.
6. PERFORMING ORG. REPORT NUMBER
7. AUTHOR(s): Randolph L. Carlson
8. CONTRACT OR GRANT NUMBER(s)
9. PERFORMING ORGANIZATION NAME AND ADDRESS: Air Force Weapons Laboratory (ALC) Kirtland Air Force Base, New Mexico 87117
10. PROGRAM ELEMENT, PROJECT, TASK AREA & WORK UNIT NUMBERS: 63605F AF-317J1097 10
11. CONTROLLING OFFICE NAME AND ADDRESS: Air Force Weapons Laboratory Kirtland AFB, NM 87117
12. REPORT DATE: Aug [redacted] 76
13. NUMBER OF PAGES: 54
14. MONITORING AGENCY NAME & ADDRESS (if different from Controlling Office): 12, 56p.
15. SECURITY CLASS. (of this report): Unclassified
15a. DECLASSIFICATION/DOWNGRADING SCHEDULE

16. DISTRIBUTION STATEMENT (of this Report)

Approved for public release; distribution unlimited.

17. DISTRIBUTION STATEMENT (of the abstract entered in Block 20, if different from Report)

18. SUPPLEMENTARY NOTES

19. KEY WORDS (Continue on reverse side if necessary and identify by block number)

CO_2 Laser
Electric Discharge Laser
Laser Effects

20. ABSTRACT (Continue on reverse side if necessary and identify by block number)

The optimization of a Electric Discharge Coaxial Laser (EDCL) System is described. This CW carbon dioxide laser extracts power in excess of 15 kilowatts routinely at an electrical efficiency of 25 percent and a mass flow efficiency in excess of 100 kW/lb$_m$/sec. With the appropriate resonator optics, the output intensity distribution is circular, uniform, temporarily stable, and repeatable within 5 percent. This EDCL is a high power output device offering simplicity of construction, low cost, high reliability, and ease of operation as compared to alternative transverse gas flow laser systems.

DD FORM 1 JAN 73 1473 EDITION OF 1 NOV 65 IS OBSOLETE

UNCLASSIFIED 013 150

SECURITY CLASSIFICATION OF THIS PAGE (When Data Entered)

100 kw/lb sub m/sec

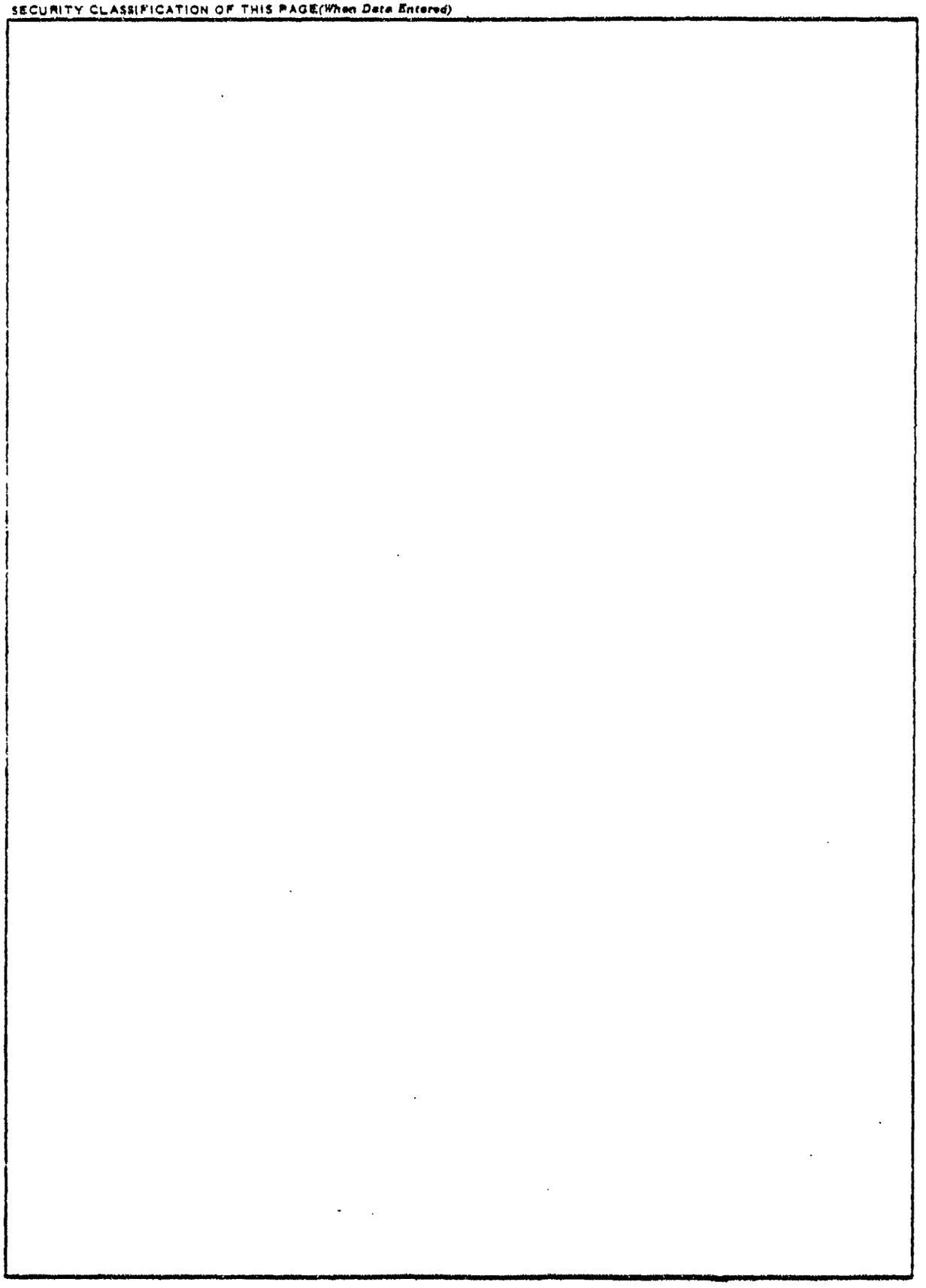

PREFACE

The author wishes to thank Sgt Michael E. Gullo for his assistance in constructing the prototype Laser System, and Sgt Robert L. Dawson for his contribution in building the present Laser Effects and Testing Facility.

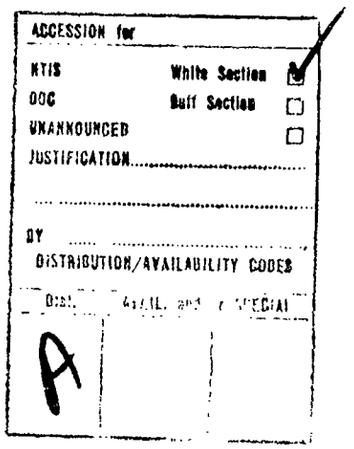

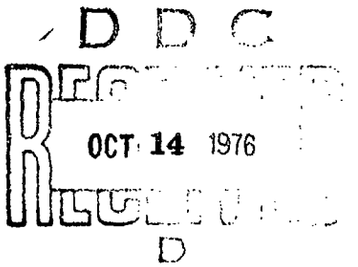

CONTENTS

ILLUSTRATIONS

SECTION I

INTRODUCTION

Since the advent of multikilowatt lasers, it has become apparent that there may be significant industrial and military applications for such laser systems. In particular, the Advanced Radiation Technology Office, Effects and Vulnerability Branch, Air Force Weapons Laboratory (AFWL), has the charter of understanding or predicting the effects of high power laser radiation on various types of materials. Much of this work is experimental in nature. Data has been obtained over the past several years on various high power laser devices which were built under developmental technology programs. Since it is desirable to perform controlled irradiations of speciman targets, a characterized and controllable laser source is required. The easiest output beam profile to employ and understand is one having a radially symmetric, uniform or gaussian intensity distribution not varying with time. The lasers built under these technology programs usually did not meet the desires of the "effects" experimenter. This led to the decision to design and construct a customized multikilowatt carbon dioxide continuous wave laser to serve as a well-characterized source of radiation for use by AFWL personnel, contractors, and other related government agencies.

The original goal was to construct a 5-kilowatt open-cycle laser system that would produce a circular and uniform intensity beam profile. After prototype studies were completed, improvements and optimization of the overall system have resulted in an EDCL which operates at a very high combined electrical and mass flow efficiency. The final device operates at a power level of 1 to 15 kW for 0 to 15 seconds with push button operation. It can be operated easily in excess of one hundred times per day. The output intensity distribution is circular and uniform, and the output power is temporally stable and repeatable within a few percent.

A duplicate of the AFWL EDCL has been constructed at the Air Force Materials Laboratory (AFML), Wright-Patterson AFB, Ohio, with consultant support from the author. Several contractors and other government agencies have expressed interest in the operating characteristics and design details of the laser. It is the intent of this report to provide open literature access to the basic engineering considerations and design approach used to develop

the AFWL EDCL. Lastly, this report provides background information for future users of the laser system at AFWL and AFML.

SECTION II

DESIGN

A logical approach is necessary to the design and engineering of a reliable high power laser. Although the context of this report covers the development of the AFWL EDCL, the fundamental design concepts are basic to all electric discharge flowing gas lasers. This section is subdivided into separate areas, but it is the combination of this information with appropiate experimentation that leads to a well-engineered laser system.

1. GAS FLOW AND VACUUM SYSTEM

The inlet gas system for the laser is shown in figure 1. The EDCL is connected to 300-psi regulated lines which come from a large tank farm. The mass flow rate of the individual gases are set by remotely loading dome regulators and reading the pressure and temperature upstream of the "choked" orifice plates. The orifices are standard sharp-edged plates with discharge coefficients of 0.60. These orifices are designed to indicate "middle of the gage" upstream pressures (readable to ± 5 percent) for the particular gas mixture used with the laser operating at the 15-kilowatt level. The carbon dioxide supply lines are preheated such that the flowing gas enters the laser at approximately 300°K. Typical total flow rates are between 0.1 and 0.2 lb_m/sec. The system is capable of flowing 0.5 lb_m/sec for each gas constituent.

As shown in figure 1, the selected flow goes through a "throttled" ball valve which opens slowly to avoid initial surges through the laser cavity. This valve is set such that the laser comes up to operating pressure within 3 seconds. The gas continues through an axial mixing chamber and feeds two axial reservoirs each made of 4 inch I.D. x 36 inch glass pipes. Each reservoir feeds four 1-5/8 inch I.D. vacuum hose lines with the gas entering each end of the laser through equally spaced coaxial ports. This entry section is described in detail later in this report. The flow continues through the laser cavity and is exhausted via a 10 inch I.D., 150-foot long line connected to a 28-foot diameter sphere. The sphere is continually pumped out by a 6000-cfm Roots blower. This vacuum reservoir is much larger than needed to operate the EDCL but was available.

The upstream pressure in the laser cavity at a given mass flow rate is controlled by adjustment of the width of the annular exit shown in figure 2. The cathode plate exit is designed to "spread" out the cathode glow over a

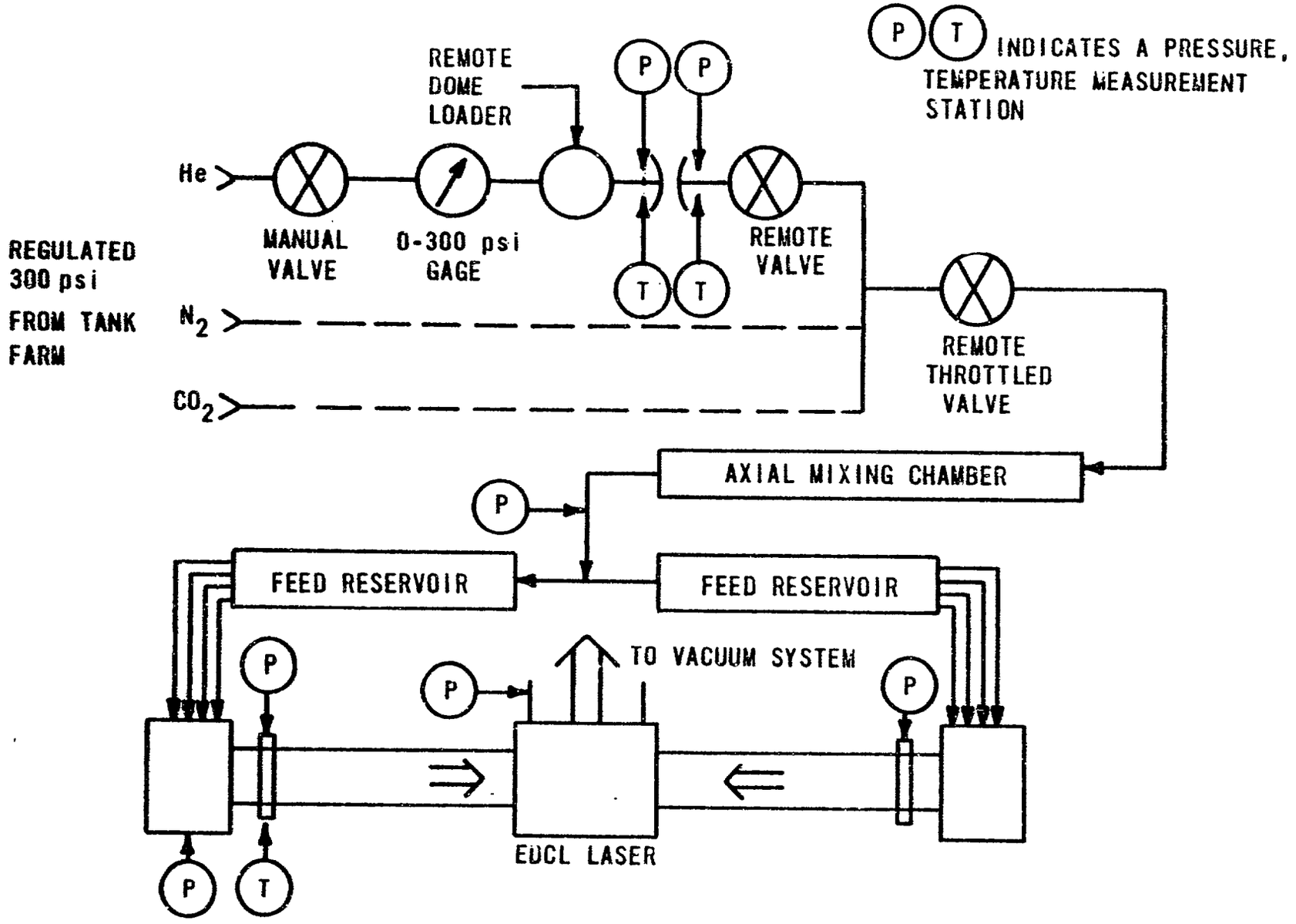

Figure 1. Laser Gas Flow System

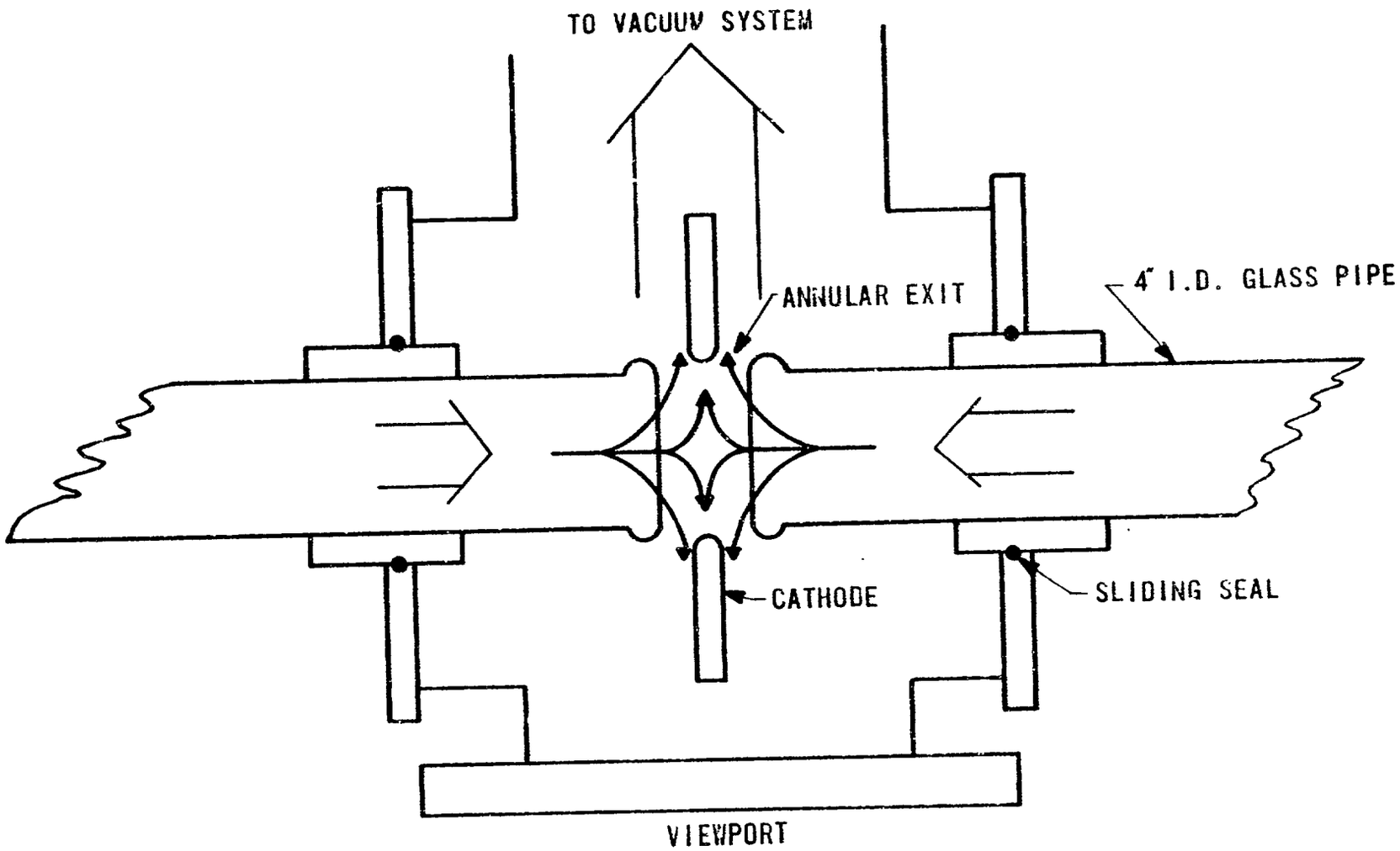

Figure 2. Laser Cavity Gas Exit System (Top View)

large uniform area for reasons described later. Since mass flow rate and upstream pressure can be controlled independently over a certain range, the capability exists to adjust the entrance Mach number for purposes of maximizing the electrical power that can be loaded into the cavity at a given mass flow rate. During no power input, the pressure drops a few percent through the laser channel. With increasing electrical power applied to the flowing gas, there is an increase in pressure drop along the laser channel. With the annular exit constriction set, the pressure at any point in the laser cavity will remain constant during gas flow until the pressure in the exhaust reservoir reaches some "critical" pressure. When the reservoir pressure increases above the "critical" pressure, the 10-inch line pressure begins to rise. A corresponding rise in the laser cavity exit pressure then occurs.

With this exit system the upstream pressure attained in the laser cavity is proportional to mass flow rate. In the absence of sphere evacuation, the sphere pressure increases proportionately with time and mass flow rate. This implies that the "critical" pressure is attained in the same maximum run time length regardless of mass flow rate through the laser. The exit of the EDCL is set at a width of about 1-3/8 inch which provided a 0 to 40 torr no-load upstream pressure for 0 to 0.2 lb_m/sec flow rate.

2. POWER SUPPLY AND CURRENT REGULATOR SYSTEM

A current regulator/ballast system is used to control the laser and keep the discharge in the glow regime. The glow discharge is characterized by a steady voltage drop along its length except for the short distance wherein the cathode fall occurs. Under these conditions, the DC voltage across the discharge is nearly independent of the DC current through the discharge. The optical output power of the laser cavity is proportional to the power input which is equal to the product of the discharge current and voltage. Since the voltage across the discharge is nearly constant with current, control of the current can be used to stabilize the output power. Furthermore, the regulator system allows each side of the laser cavity to be loaded to equal specific power inputs or independently adjusted. The regulator reduces power supply ripple, power supply turn-on transients, provides the necessary overvoltage for discharge breakdown, and represents a large positive dynamic impedance to the discharge. All of this is accomplished at minimum power dissipation in the regulator circuit.

The schematic of a regulator module is shown in figure 3 with typical operating currents and voltages. The heart of the regulator module is the high gain, wide bandwidth Eimac 8166 tetrode which contains a regulated, self-biased screen and variable grid supply. The ten-turn potentiometer is used to set the DC current value over the range of approximately 0.2 to 0.8 amp. At the plate to cathode voltage of 2500, the tube dissipation varies from 500 to a maximum of 2000 watts. Although 2000 watts exceeds the tube ratings by a factor of two, the plate mass is sufficient to easily satisfy the plate temperature requirements for a 15-second run.

Three modules in parallel per laser side are connected to the laser cavity as shown in figure 4. The three regulator modules are connected to the positive output of a Hipotronics Model 825-4.5A, 0 to 25 kV, 0 to 4.5 amp power supply. The output of the regulators (A') are connected to 16 (20 kilohm) ballast resistors which feed one side of the laser. These ballast resistors divide the regulated current equally between the 16 electrodes and provide the discharge anodes a limiting resistance in case of a tube failure. All bias, meter, and tube currents are summed to feed the ballast resistors maximizing the use of available electrical power deliverable to the laser cavity by the power supply.

The effectiveness of the regulator in controlling a possible fluctuating discharge impedance is analyzed by reviewing the equivalent small signal, audio frequency circuit shown in figure 5. R is the parallel combination of either five or six 20K ballast resistors, v_d is the incremental discharge voltage which is a function of i, and v_s is the power supply ripple. The following equations may be written from figure 5:

$$i_1 = \frac{v_s - v_d - (i_1 + i_2) R_k - iR + \mu e_g}{r_p} \qquad (1)$$

$$i_2 = \frac{v_s - v_d - (i_1 + i_2) R_k - iR}{R_s} \qquad (2)$$

$$i_3 = \frac{v_s - v_d - iR}{R_g} \qquad (3)$$

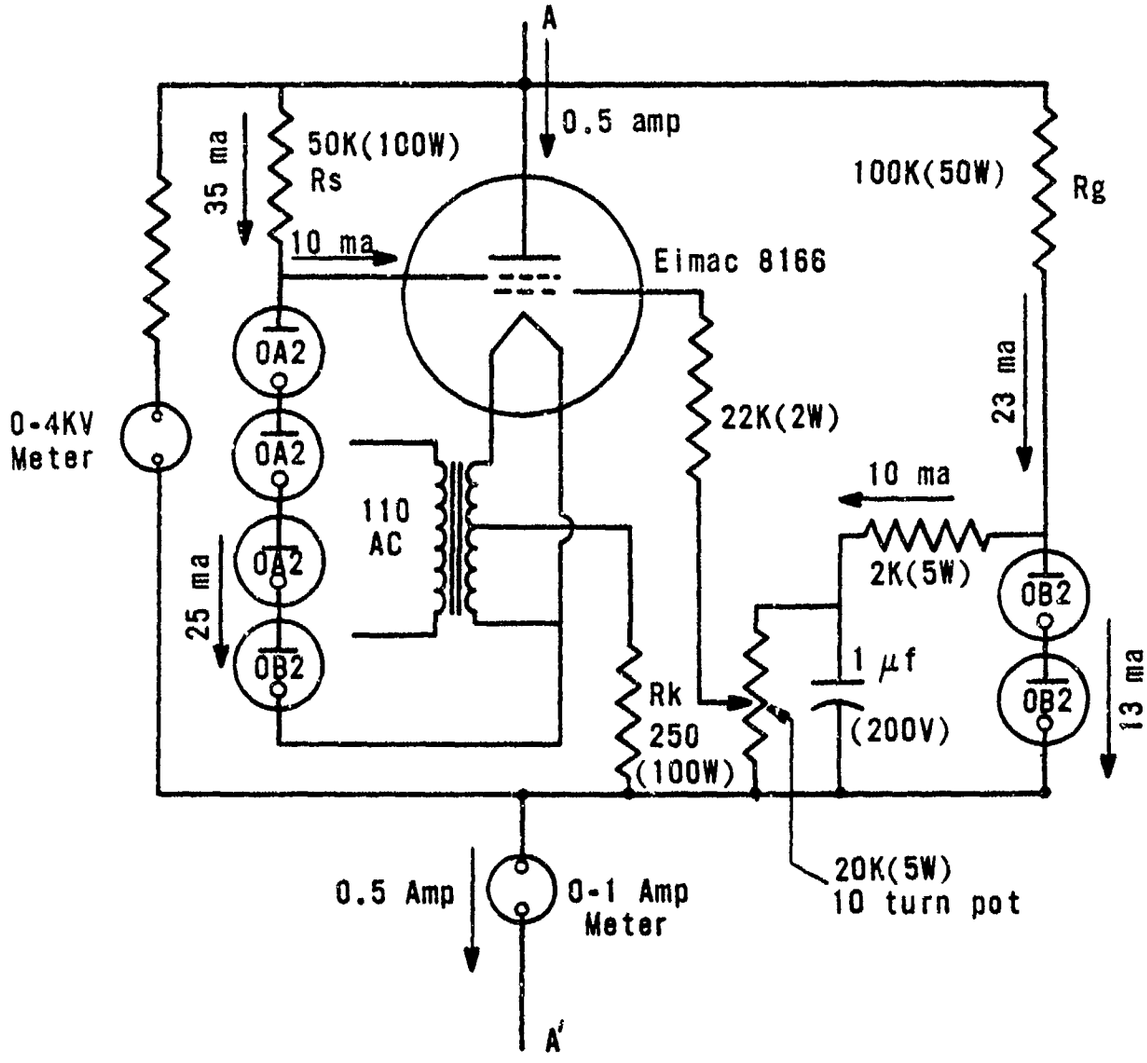

PLATE VOLTAGE (A-A') ≈ 2500

SCREEN VOLTAGE ≈ 555

VARIABLE GRID VOLTAGE ≈ 0 to 180

Figure 3. Regulator Module

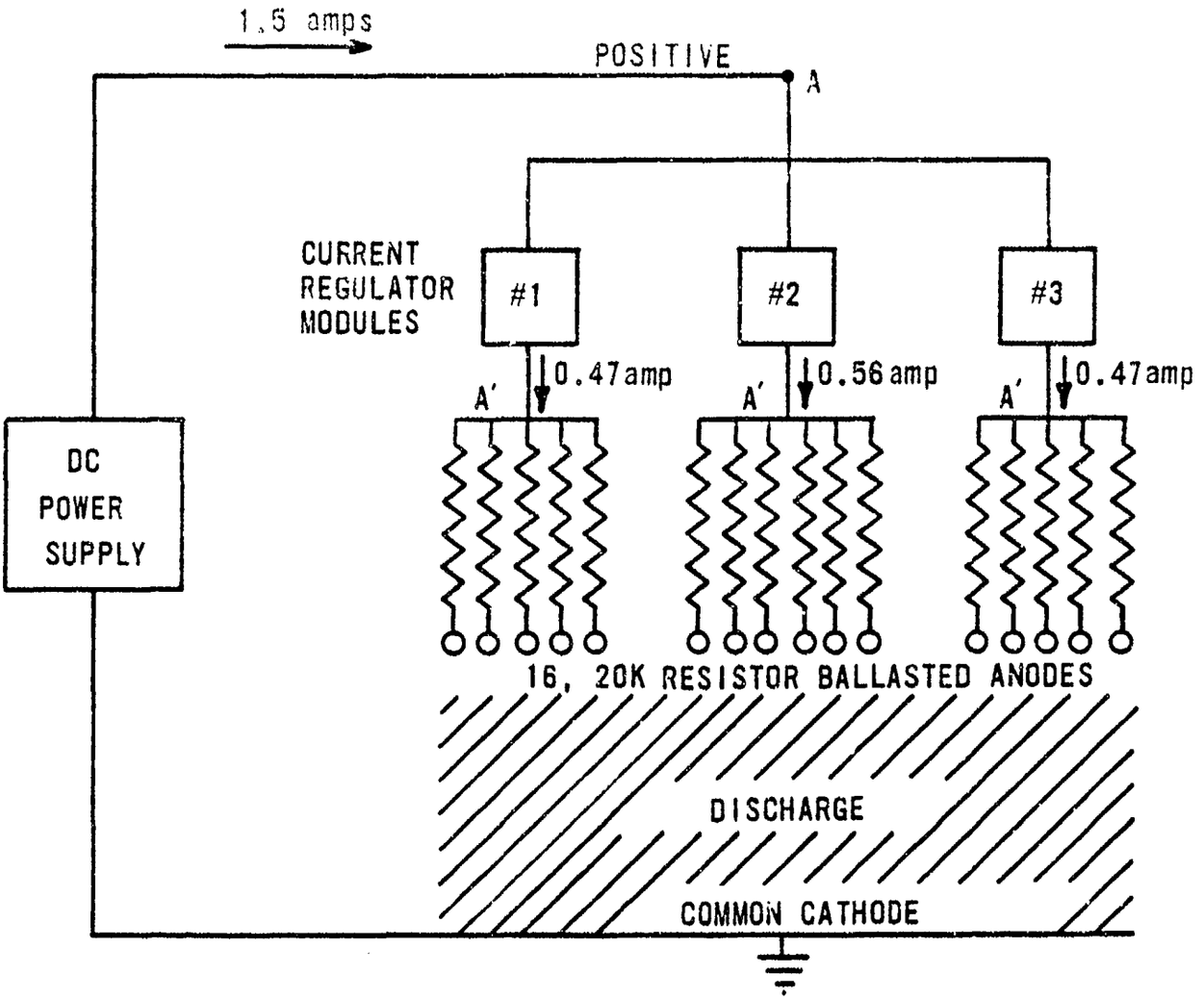

Figure 4. Power Supply Distribution System (One Side of Laser)

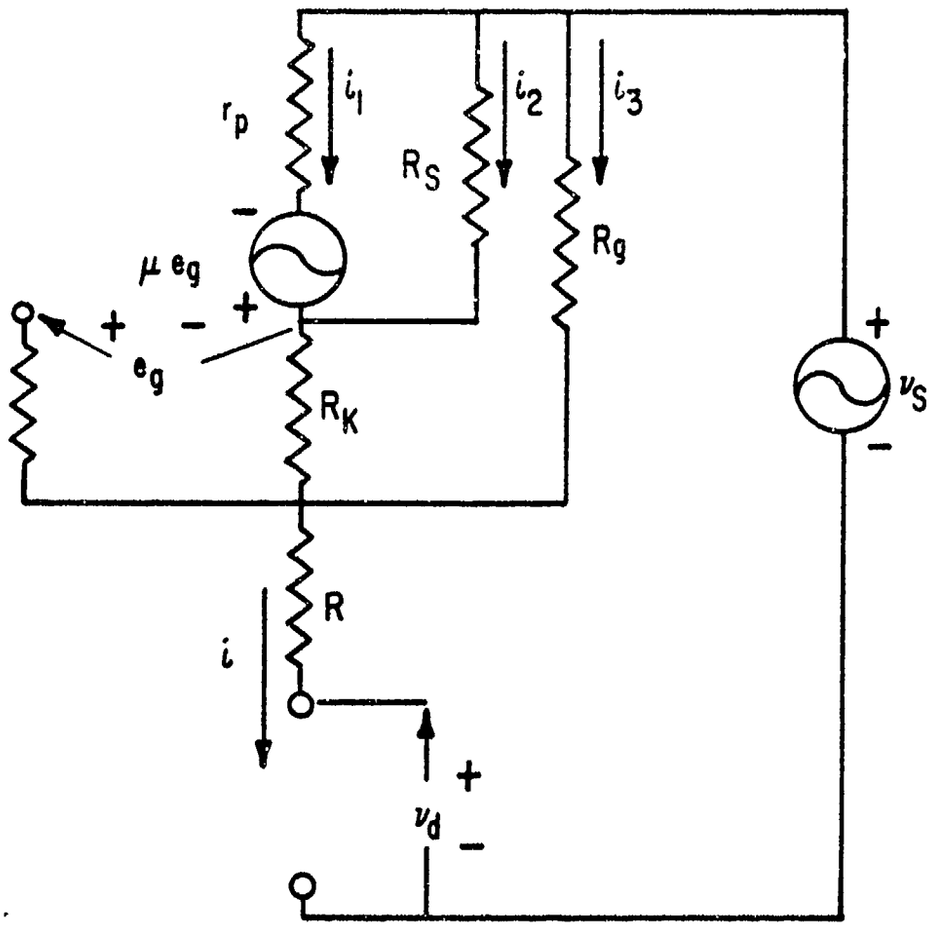

$r_p \approx 20K$

$\mu \approx 200$ to 300

Figure 5. Small-Signal Regulator Equivalent Circuit

$$e_g = -(i_1 + i_2)R_k \tag{4}$$

$$(\mu + 1) \simeq \mu \tag{5}$$

$$i = i_1 + i_2 + i_3 \tag{6}$$

Solving for i, we get

$$i = \frac{(v_s - v_d)(a + 1/R_g)}{1 + R(a + 1/R_g)} \tag{7}$$

where

$$a = \frac{(1/r_p + 1/R_s)}{(1 + R_k(\mu/r_p + 1/R_s))}$$

For purposes of easier analysis we set $R_g = R_s = \infty$, then

$$i = \frac{v_s - v_d}{R + (\mu R_k + r_p)} \tag{8}$$

The simplest case describing the glow discharge assumes that the change in discharge voltage is proportional to the change in discharge current. The DC discharge voltage (V_D) as a function of DC discharge current (I) is:

$$V_D = V_{DO} + I\, r_d \tag{9}$$

where r_d = slope of voltage/current characteristic of discharge, and V_{DO} = discharge voltage for current equal to zero. The differential change in V_D as a function of changes in V_{DO} and I is given by

$$dV_D = \frac{\partial V_D}{\partial V_{DO}} dV_{DO} + \frac{\partial V_D}{\partial I} dI \tag{10}$$

Using the definition of an incremental variable and equation (9) gives

$$v_d = v_{do} + r_d\, i \tag{11}$$

where

$dV_D \equiv v_d$ = incremental discharge voltage at any current I

$dV_{DO} \equiv v_{do}$ = incremental discharge voltage at current I = 0

$dI \equiv i$ = incremental discharge current

The change in regulator current is then given by

$$i = \frac{v_s - v_{do}}{R + (\mu R_k + r_p) + r_d} \tag{12}$$

The term $(\mu R_k + r_p)$ represents the dynamic positive impedance contributed by the 8166 regulator. A positive discharge impedance ($r_d > 0$) aids in reducing the current variation whereas a negative impedance ($r_d < 0$) has the opposite effect. In the absence of the large positive regulator term $(\mu R_k + r_p) >> R$, it is possible for $(R + r_d)$ to approach zero. This could lead to variations in i which can cause the discharge to go irreversibly into a form of discharge known as the arc regime. From equation (12) it is evident that the effect of the regulator is to reduce power supply ripple and provide closed loop negative feed back on discharge conditions. For example, an incremental decrease in discharge impedance tends to cause an increase in current (i). The action of the regulator is to reduce the voltage (v_d) hence reducing the current (i) to its original valve. The regulator converts the unregulated power supply voltage source into a controlled current source.

For three identical modules in parallel feeding five ballast resistors each, the total incremental current (i_t) is

$$i_t = \frac{3(v_s - v_d)\ (a + 1/R_g)}{1 + R(a + 1/R_g)} \tag{13}$$

For the component values shown in figure 5 and using a nominal value for μ of 250, equation (13) becomes

$$i_t = 0.07(v_s - v_d) \tag{14}$$

where (i_t) is in amps and (v_s, v_d) are in kilovolts.

Given a total DC current of 1.5 amps it can be shown that the regulator provides a factor of five reduction in current variation as compared to a fixed resistor ballast of equal power dissipation. An externally biased regulator approaches the condition of $R_g = R_s = \infty$ and equation (8) for three regulator modules predicts $i_t = 0.035(v_s - v_d)$. A factor of two improvement in regulation could be achieved at a small sacrifice in circuit complexity by providing separate regulated voltage supplies for the screen and grid circuit.

Significantly greater reduction in discharge current fluctuation is not easily attainable without some added sophistication to the regulator module of figure 5. One such change would require the use of separately regulated screen and grid supplies. The cathode resistor (R_k) is replaced by the collector-emitter terminals of a high power transistor with its base driven by a variable current source. The dynamic collector impedance (several hundred of kilohms) is then multiplied by the (μ) of the tube. This type of circuitry is capable of reducing current variations by several orders of magnitude, but is considered an unnecessary complexity in the present application.

Turn-on transients from the power supply are eliminated by the equivalent RC network in the grid circuit. These events are depicted in figure 6. At power supply turn-on, the 1μf capacitor shown in figure 3 is uncharged, causing the grid to be grounded. The tube current increases initially to satisfy the voltage, current, and grid characteristics of the tube for the grounded grid condition. The capacitor then charges with a time constant of approximately 9 milliseconds toward the final grid voltage value and hence final tube current value.

3. LASER CAVITY WITH POWER LOADING

Electrical power applied to the flowing gas in the cavity is distributed in the forms of gas heating, acceleration of the gas, laser radiation, spontaneous emission, and diffusion losses to the cavity walls. Assuming that these last two mechanisms are negligible and that the output laser radiation can be represented by a uniform fractional loss (n) of the electrical power input (P_e), the power input (P_g) to the gas is $P_g = (1 - n)P_e$. For the case of a radially uniform heat input to a flowing gas in frictionless, constant area duct, the parameters of pressure (P), temperature (T), density (ρ), velocity (V), and Mach number (M) are related by the compressible flow equations describing Rayleigh Line heating (ref. 1).

$$\frac{P_2}{P_1} = \frac{1 + \gamma M_1^2}{1 + \gamma M_2^2} \tag{15}$$

$$\frac{T_2}{T_1} = \left(\frac{P_2}{P_1}\right)^2 \left(\frac{M_2}{M_1}\right)^2 \tag{16}$$

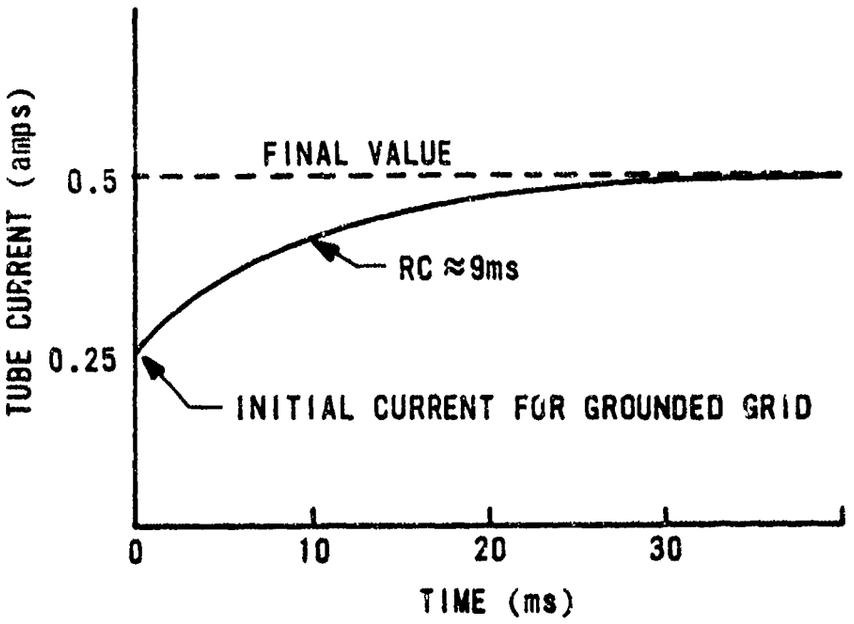

Figure 6. Transient Current Suppression

$$\frac{\rho_2}{\rho_1} = \frac{V_1}{V_2} = \left(\frac{P_2}{P_1}\right)\left(\frac{T_1}{T_2}\right) \tag{17}$$

where γ is the ratio of specfic heats (C_p/C_v) and the subscripts (1, 2) refer to upstream and downstream conditions, respectively.

The power input (P_g) to the gas is related to the increase in total temperature (T_o) by

$$P_g = \dot{m}C_p(T_{o2} - T_{o1}) \tag{18}$$

where $T_{oi} = T_i\left(1 + \frac{\gamma - 1}{2} M_i^2\right)$ and $\dot{m}$ = mass flow rate (lb_m/sec).

Once a specific gas mixture has been selected, γ and C_p are fixed. It is then desirable to maximize the specific power input ($P_g/\dot{m}$) under constraints imposed by exit Mach number, maximum temperature in the laser channel, and pressure ratio along the cavity. These parameters can be controlled by adjusting the entrance Mach number and the electrical power input to the gas.

Equations (15), (16), and (18) can be solved simultaneously for entrance Mach number (M_1) with ($P_g/\dot{m}$) and (M_2) as variables. The solution of these equations is facilitated by introducing ratios of the total temperature to the total temperature that would exist at M = 1 (ref. 1).

$$\frac{T_{o1}}{T_o^*} = \frac{2(1 + \gamma)M_1^2}{(1 + \gamma M_1^2)^2}\left(1 + \frac{\gamma - 1}{2} M_1^2\right) \tag{19}$$

$$\frac{T_{o2}}{T_o^*} = \left(\frac{P_g}{\dot{m}C_p T_{o1}}\right) + 1\left(\frac{T_{o1}}{T_o^*}\right) \tag{20}$$

$$M_2^2 = \frac{1 - \left[1 - \frac{T_{o2}}{T_o^*}\right]^{1/2}}{1 + \gamma\left[1 - \frac{T_{o2}}{T_o^*}\right]^{1/2}} \tag{21}$$

where T_o^* = total temperature at M = 1. Equations (19), (20), and (21) are solved sequentially for M_2 given $P_g/\dot{m}$ and allowing M_1 to be a variable. M_1 and M_2 are then used with equations (15) and (16) to calculate T_2. A family of curves showing exit temperature versus entrance Mach number with $\gamma = 1.56$, $T_1 = 300°K$, and $C_p = 1000$ joules/lb_m °K is shown in figure 7 for several specific input powers. At a given specific power input, the temperature decreases as the input Mach number is increased until the exit Mach number equals unity as indicated by the ending of the curves toward the right side of figure 7. If conditions are such that the exit Mach number is near unity, the maximum temperature in the channel is attained at a position corresponding to $M = 1/\sqrt{\gamma}$ from equation (16). The temperature at $M = 1/\sqrt{\gamma}$ versus entrance Mach number is overlayed on the plot. Since the fractional population inversion of the laser medium starts to decrease significantly for temperatures greater than about 550°K (ref. 2), then at a fixed entrance Mach number the electrical to optical extraction efficiency will decrease for further increase in specific power input. Hence, the $M = 1/\sqrt{\gamma}$ curve gives the required entrance Mach number ($M_1 \approx 0.35$) and the maximum specific input power ($P_g/\dot{m} \approx 350$ kW/lb_m/sec) that can be put into the gas up to the position corresponding to $M \approx 1/\sqrt{\gamma}$ in the laser channel. Additional input power can be added until the Mach number is increased from $M = 1/\sqrt{\gamma}$ to M = 1 with a corresponding temperature decrease at the exit.

Figure 8 displays the Mach number, temperature, pressure, density, and velocity ratios versus cavity length for $\gamma = 1.56$, $M_1 = 0.35$, and $P_g/\dot{m} = 350$ kW/lb_m/sec. These curves are generated by incrementing M_2 from $M_2 = M_1 = 0.35$ to $M_2 = 1$ in equation (18) with P_g replaced by the fractional cavity power $(X/L)\,P_g$. The abscissa of figure 8 may also be interpreted as the fractional amount of $P_g/\dot{m} = 350$ kW/lb_m/sec that has been added to the flowing gas. Using this interpretation, it is noticed that the curves continue beyond X/L = 1 indicating that an additional power of 18 kW/lb_m/sec can be added until $M_2 = 1$. If the selected initial conditions were $P_g/\dot{m} = 368$ kW/lb_m/sec, $\gamma = 1.56$, and $M_1 = 0.35$, then the curves would terminate at X/L = 1. The peak in the temperature profile is seen to occur near the exit of the laser cavity.

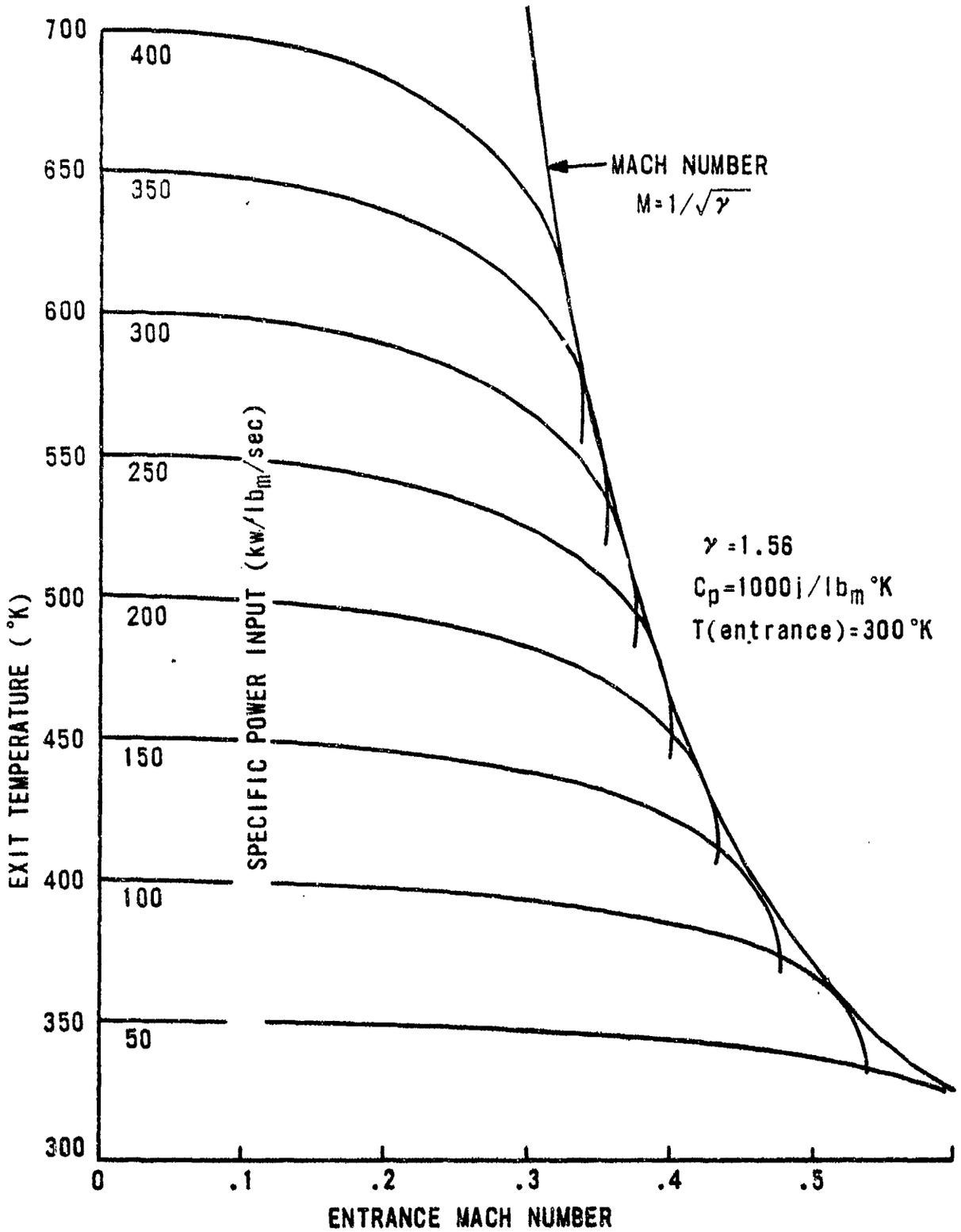

Figure 7. Exit Temperature Versus Entrance Mach Number

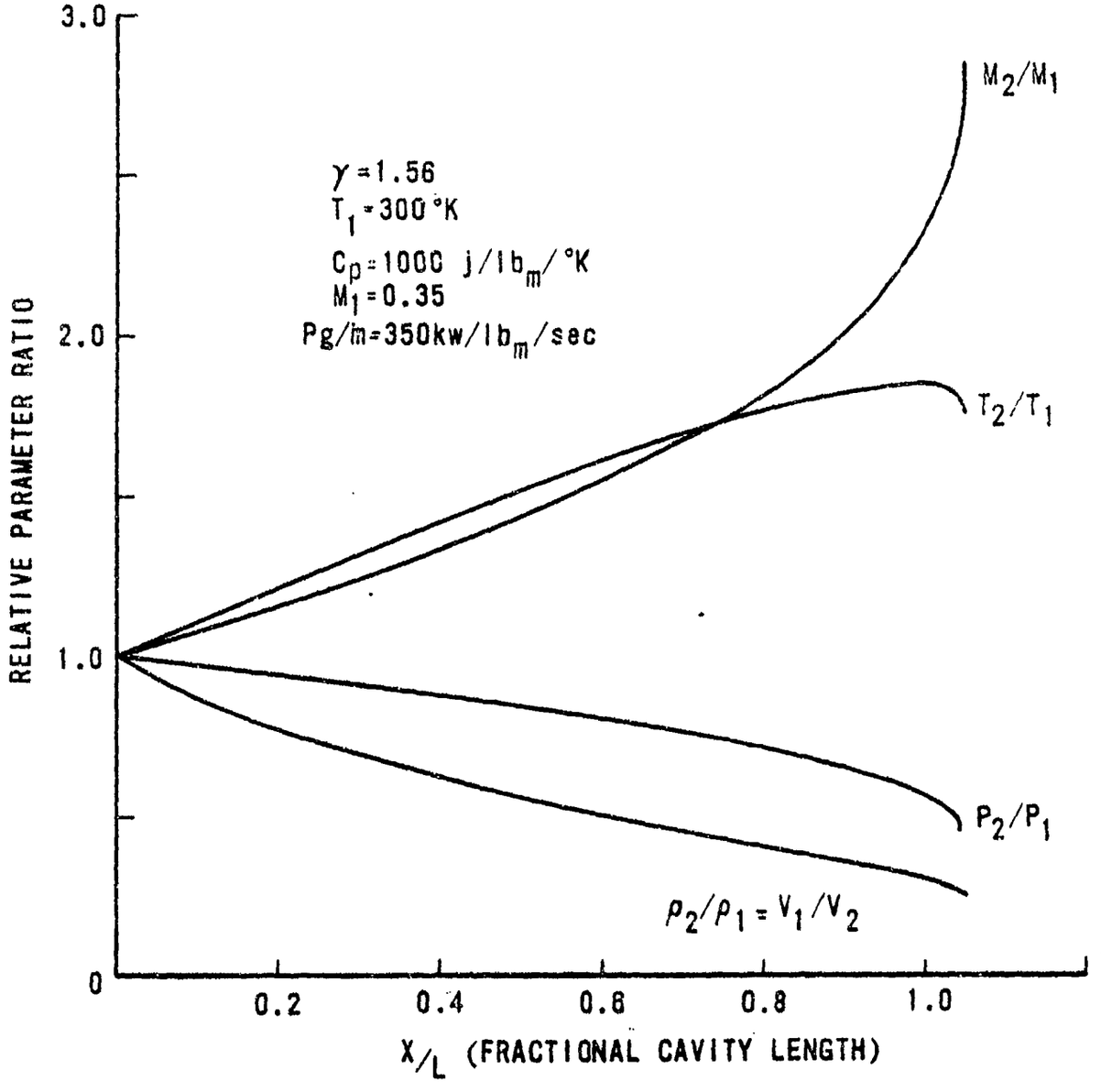

Figure 8. Laser Cavity Parameters Versus Fractional Cavity Length

It is observed that the maximum density ratio along the channel is about 4 to 1 for the above given conditions. As discussed in the next section, the decrease in density toward the laser exit under the conditions of uniform power loading with length can lead to downstream localized regions wherein the electric field per electron number density increases toward a critical value. Above this critical value these regions can cause streamers in the gas which might propagate upstream to the anodes with the result that the uniform glow discharge goes irreversibly into the arc discharge. Review of equation (17) indicates that this density ratio is controlled by the ratio of M_2 to M_1 and the particular value of M_1. The temperature, density, and Mach number ratios are near optimum for the stated entrance Mach number of 0.35 and specific input power of 350 kW/lb_m/sec. The design of the EDCL cavity is such that nearly all power applied to the flowing gas discharge is available for extraction by the resonator optics.

4. LARGE VOLUME UNIFORM ELECTRICAL DISCHARGE

To load up to 75 kW of electrical power into the EDCL cavity, large volume, fast-flow discharge techniques are required to produce a uniform discharge of high stability. This task is achieved in higher pressure and larger laser devices using such sources of preionization as electron beam injection, ultraviolet photoionization, and other advanced techniques (ref. 3). These approaches are complex and costly. An alternative approach utilizing aerodynamic forces to control the upstream ion distribution has also been successful (ref. 4) for laser discharges operating below 50 torr. This technique was chosen for the AFWL EDCL.

A single anode-cathode column discharge operating in the "normal" glow regime is characterized by ions leaving in the vicinity of the upstream anode drifting downstream toward the cathode while drifting radially outward from the hot discharge center. The "normal" glow regime is defined as that portion of the voltage/current characteristic of a discharge wherein the voltage across the discharge is nearly independent of the current through the discharge. The current density of such a discharge is limited in stability due to thermal gradients imposed by nonuniform electrical conductivity which is caused by the radially diffusing ions and a decrease in gas density on the discharge axis. A further increase in discharge current above the "normal" glow regime is termed the "abnormal" glow and is further characterized by a

concentration of current along the discharge axis. At some critical value of increasing current, the discharge switches abruptly and regeneratively into the "arc" regime which is characterized by very high discharge current and essentially zero discharge voltage. Hence, there exists a finite current region over which the discharge has a diffuse glow and can be used for laser mode volume excitation. Many discharge columns can be combined in various arrays to give a large volume discharge of yet still limited stability.

An array of discharge columns can be made more stable by tailoring the upstream ion distribution by techniques used in the electro-aerodynamic laser (EAL) (ref. 5). In this device, it has been demonstrated that aerodynamic pressure gradients can have a pronounced affect on upstream ion motion which in turn can control the discharge current density profile. Since e drift velocity of the electrons is many times greater than that of the ions, the current is carried by the electrons. The requirement of charge neutrality in the positive column of the discharge implies that a controlled upstream ion distribution might affect the drifting electron distribution and hence the spatial distribution of the discharge current density.

The upstream electrode and gas entrance section of the EDCL is shown in figure 9. The inlet gas is distributed into an annulus via the four equally spaced entrance ports (only two are shown for clarity) and moves downstream across the anodes and into the laser cavity. The dimensions and shape of the entrance section near the anodes is such that a pressure gradient radially inward is imposed on newly created ions. These aerodynamic forces are portrayed by the sequence of vectors superimposed on a hypothetical ion trajectory. Each anode is bullet-shaped and acts as its own generator of turbulence to aid in diffusing created ions into the regions of aerodynamic forces dictated by the entrance section. Each end of the EDCL has 16 anodes placed in an annular array with the optical mount attached coaxially to the upstream end of the electrode section. Although not used in the final EDCL design, the possibility of installing an annular array of dielectric nozzles or vanes upstream of the anodes considered. This arrangement could be used to introduce additional turbulence in the vicinity of the anodes. The inlet of the EDCL would then be similar to that of the EAL in providing an additional means of diffusing the upstream ion distribution.

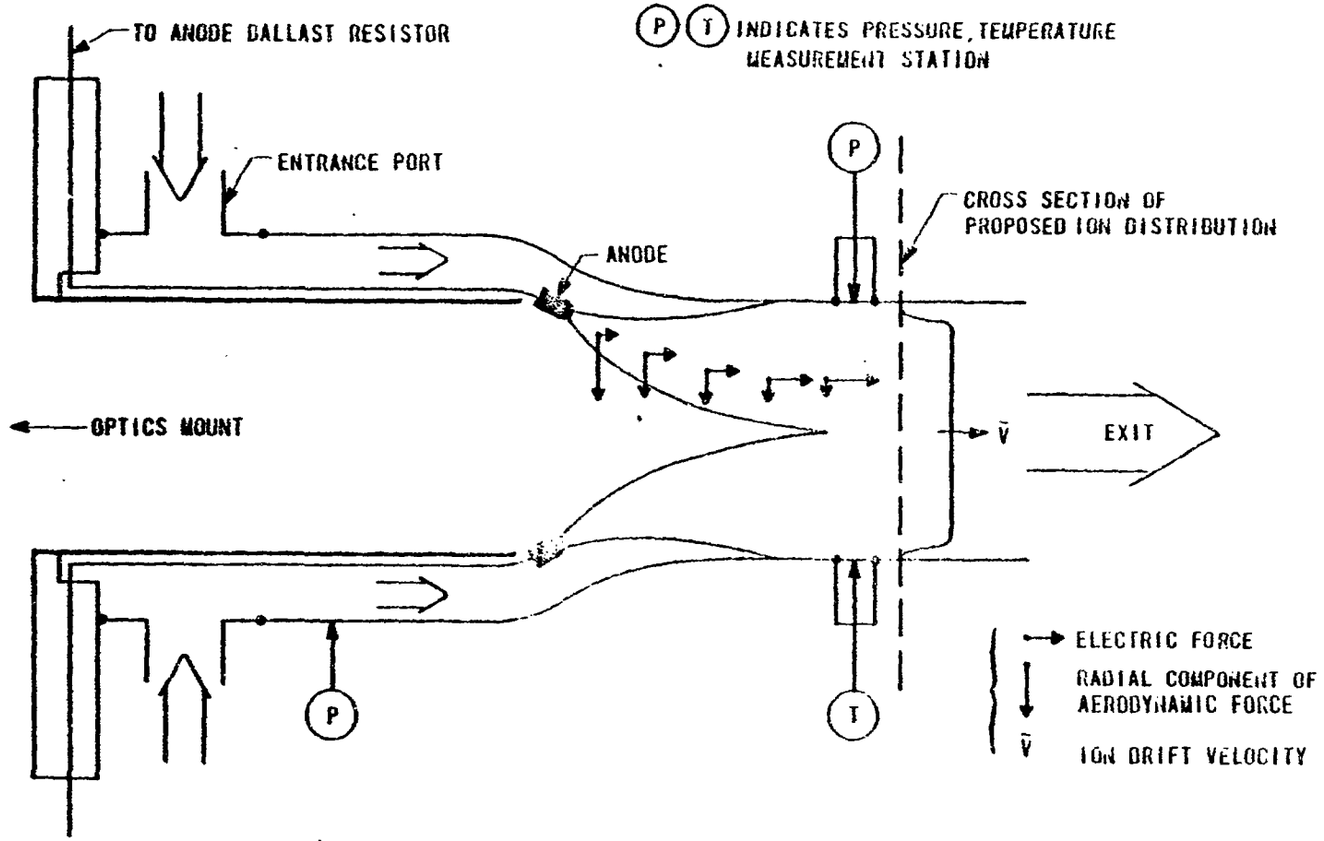

Figure 9. Electrode Structure

The present electrode structure causes the 16 columnar discharges to merge into a single uniform discharge after a distance of about 10 cm of downstream travel. Pictorially, figure 9 shows the proposed ion distribution which in turn tailors the upstream drifting electron (hence current density) distribution. The uniform discharge created after this initial 10 cm remains stable and uniform for 0.8 meter of cavity length.

The exact number of electrodes used in the EDCL was experimentally chosen subject to the following concepts. There exists some current above which an individual anode-cathode discharge will go unstable into the arc discharge. The maximum total discharge current is a function of the number of anodes in a discharge array given a cathode of sufficient area. Current capability continues to increase with additional electrodes until the distances between anodes allows newly created ions from one anode to diffuse and merge with the ions of an adjacent anode. The anodes no longer appear as separate sources of ions in thermal equilibrium with the entering gas flow and the discharge arcs.

There are two additional effects that can cause the discharge to become unstable. If the gas exchange time is too long (slow flow lasers), severe thermal disturbances and gradients can be created locally in the discharge. A high velocity flow with introduced turbulence in the gas tends to spatially average out these localized disturbances. Secondly, in long lasers the effects of the electric forces can overcome the entrance aerodynamic forces used to create the discharge uniformity with the result that after some distance downstream, the discharge separates back into individual columnar discharges. Insufficient gas velocity and entrance forces can cause the desired glow discharge to transform into the arc discharge at higher specific power inputs. The EDCL cavity is short enough and the entrance Mach number is high enough that these effects do not occur for specific power inputs to the gas of up to 360 $kW/lb_m/sec$ over the pressure region of 10 to 35 torr.

As mentioned in section II.1, the negative electrode (ground) had sufficient area that the cathode glow gradually increased in area to cover the cathode plate within the current limits of the available power supply. The annular gas exit aids in sweeping away any localized thermal disturbances in the cathode fall region which could lead to regions of high current density and resultant arcing. Assuming that the gas exit is not already sonic, increasing the power input at a given mass flow rate decreases the density

towards the cathode exit. This reduced density under the nearly uniform potential gradient across the discharge can lead to a significant increase in electric field per electron number density (E/N in volts-cm^2/electron) near the channel exit.

As the E/N is increased above some critical value, the glow discharge breaks down into filamentary streamers which can then propagate across the discharge electrodes. This results in the discharge switching to the region of higher conduction in a regenerative fashion such that the discharge goes irreversibly into an arc. In a transversely excited laser with a single anode and cathode, the increased E/N near the gas exit occurs between and in the vicinity of both electrodes. Hence, discharge stability becomes a critical function of the local E/N in the region near the exit.

The EDCL flow is colinear with the electric field and the gas exits across and in the vicinity of only one electrode. It is conceptually possible to have a local increase above the critical E/N near the cathode of the EDCL, and although short streamers form near the cathode, the remainder of the discharge having a lower E/N acts as a ballast in preventing total discharge instability.

For personnel safety and simplicity of high voltage engineering, it was decided to limit the voltage across the laser cavity to 20 kilovolts. For typical CO_2 laser gas mixtures encountered in pratical low pressure devices, the average electric field per torr of gas (E/P in volts/cm-atm) is about 4500 to 5500 volts/cm-atm. A maximum cold flow cavity pressure of 40 torr and a nominal E/P of 5000 volts/cm-atm limits the cavity length to ≈ 75 cm. A prototype of the EDCL has demonstrated that this length is also near optimum for high power discharge operation and provides sufficient gain-length for efficient optical extraction.

5. RESONATOR OPTICS

A uniform circular output beam profile was required, and it was desirable to obtain this beam profile at high combined electrical and mass flow efficiency to reduce gas handling costs of an open-cycle system. With the advent of large, low loss, high power window materials at reasonable cost, the stable resonator operated in a multi-mode configuration can satify the above requirements.

A review of references 6 and 7 indicates that a stable high Fresnel number (long radius optics) resonator will operate at very low intracavity loss in

a diffuse multimode manner. The EDCL resonator consists of a 15-meter radius, 4.5-inch diameter Be-Cu mirror coated with Ag plus a protective layer of ThF_4, and a flat, 4.5-inch diameter ZnSe output coupler. The output coupler has a nominal 75 percent reflective coating on the cavity side and an antireflective coating on the outside. Previous experience indicates that optical components that are similar to the mirror and output coupler absorb and scatter less than 1 percent of the energy incident on the reflective coatings. The output coupler has a total attenuation of 2.5 percent. The mirror radius was chosen to be as long as possible without introducing appreciable diffraction losses and mechanical alignment stability problems. Usually this requirement constrains the radius of curvature to be not greater than 10 times the mirror-window separation.

To extract power at the highest efficiency, the parameters of cavity length, coupling coefficient, gas mixture, and electrical power loading must be optimized. Subsections 3 and 4 define the requirements for maximum power input to the gas in terms of cavity length, pressure, and temperature limits. The overall system efficiency (n_{tot}) can be expressed as

$$n_{tot} = n_q n_m n_p n_{elect} n_{ext} \tag{22}$$

where

n_q = fractional quantum efficiency = 0.41

n_m = 1 - (fractional loss through output coupler)

n_p = fractional mode volume available for optical extraction

n_{elect} = fractional electrical to upper laser level coupling efficiency

n_{ext} = fractional output power extraction efficiency

The n_{ext} term will be shown to be the fraction of available laser energy extracted per unit volume and is a function of cavity losses, coupler transmission, and the gain-length product of the laser cavity. The other terms n_m, n_p, and n_{elect} can be near unity with the proper gas mixture and choice of optical components. Rigrod (ref. 8) derives an expression for the radiation intensity obtainable from lasers with homogeneous line broadening under the

condition that the cavity losses are uniformly concentrated at the resonator mirrors and that the gain coefficient (related to population inversion) is isotropic and does not change with time.

Rigrod's expression modified for a resonator with a mirror of transmission t_1, coupler transmission of t_2, and optics losses of a_1 and a_2, respectively, gives:

$$I_o/I_s = \frac{t(1-a)^{1/2}\left(g_o L + \ln\left[(1-a)^{1/2}(1-a-t)^{1/2}\right]\right)}{(1-a)^{1/2}(a+t) + a(1-a-t)^{1/2}} \qquad (23)$$

where: $t_1 = o$

$t_2 = t$

$a_1 = a_2 = a$

I_s = saturation intensity (watts/cm^2)

I_o = output intensity (watts/cm^2)

t = coupler transmission

g_o = unsaturated gain coefficient (cm^{-1})

L = active laser length (cm)

a = fractional absorptive plus scatter losses of optics

The extraction efficiency, n_{ext}, is defined as

$$n_{ext} \equiv \frac{P_{out}}{P_{max}} \qquad (24)$$

where P_{out} is the extracted laser power for the given resonator conditions, and P_{max} represents the maximum output power that could be obtained with the oscillator considered as a single-pass, highly saturated amplifier. For a medium with homogeneous line broadening, the net gain coefficient, g(z), as a function of position, z, in the oscillator is related to the forward saturation intensity, I^+, growth by (ref. 8):

$$g(z) = g_o(1 + I^+/I_s)^{-1} = \frac{1}{I^+}\frac{dI^+}{dz} \qquad (25)$$

The maximum power output is determined by integrating this expression over the gain length, L, as I^+/I_s approached infinity.

$$\int_0^L g_o dz = \lim_{I^+/I_s \to \infty} \int (1 + I^+/I_s) \frac{dI^+}{I^+} \tag{26}$$

By definition, I^+ approaches the maximum output intensity, I_{max}, of the laser when I^+/I_s approaches infinity. The maximum output power, P_{max}, is then equal to the cross sectional cavity area multiplied by I_{max}, that is,

$$P_{max} = AI_{max} = I_s A g_o L = g_o I_s V \tag{27}$$

where A is the cross-sectional cavity area and V is the cavity volume. Hence, the extraction efficiency represents the fraction of maximum volumetric laser power that is extractable with a given resonator. Using the definition for n_{ext} and the Rigrod intensity expression with $P_{out} = AI_o$, we note that n_{ext} approaches unity as $g_o L \to \infty$ and $a \to 0$, regardless of the coupler transmission. Generally, a laser is said to be "saturated" when the output power does not appreciably change for wide variations in output coupler transmission.

The gain coefficient for a smaller EDCL using typical laser mixtures operating in the region of 20 to 40 torr was measured to be about 1.0 to 0.5 percent/cm (ref. 9). Since the gain (g_o) is a function of pressure, it is dependent upon laser channel position, flow velocity, and temperature. The Rigrod expression, equation (25), gives a first order estimate of intensity distribution assuming some average value of gain (g_o) along the cavity length of the EDCL discharge. Cavity lengths made up of standard 24- or 30-inch pipe sections plus the electrode assembly and gas exit gave maximum possible active cavity lengths of 150 to 180 cm, respectively. As was mentioned earlier, the 16 electrodes create upstream ionized columns which aerodynamically merge into a uniform discharge after about 10 cm of downstream travel. This 10-cm upstream region is heated to a higher temperature than in the uniform discharge due to the concentrated column discharges near the anodes not utilizing all of the gas flow cross-sectional area. Hence, neither the actual gain nor the active cavity length are accurately known. However, the effective gain length product must lie between the limits of 0.75 to 1.8

based upon possible active cavity lengths and estimated range of gain (ref. 9).

Using the ratio of equation (23), with $P_{out} = AI_o$, and equation (27); the extraction efficiency, equation (24), is plotted in figure 10 as a function of coupler transmission, cavity loss of 0.01, and a family of gain length products from 0.5 to 2.0. The optimum coupler transmission lies between 0.1 to 0.3 for the 4 to 1 range of gain length products with the corresponding extraction efficiency between 0.74 to 0.86. Thus, a good choice of output coupler transmission giving an η_{ext} of about 0.8 can be chosen from figure 10 with little knowledge of the exact gain length product. Although not shown in this plot, the optimum coupler transmission for a given g_oL shifts toward higher transmission for increasing cavity losses and higher cavity losses correspond to lower extraction efficiences. For example, if $g_oL = 1$ and $0.005 < a < 0.02$, then $0.86 > \eta_{ext} > 0.73$ and $0.12 < t$ (optimum)< 0.2.

Normally a probe laser is used to measure the gain (g_o) or it can be calculated by various laser kinetics codes. The Rigrod expression gives a good estimate of the optimum output coupler transmissions for a stated gain (g_o). The appropiate probe laser was not available; however, two output couplers having different transmissions were used to solve the Rigrod expression, equation (23), for an effective (g_oL) at a particular specific power input. The two different output couplers were fabricated from germanium blanks. Both couplers had an antireflective coating on one side; the other side of one coupler was uncoated and the second coupler was coated for a 71 percent reflectivity. Spectrophotometer measurements of coupler transmission indicated that there was a 4 percent absorption in the bulk with an additional 2 percent absorption and scatter throughout the coatings and substrate.

Initially the EDCL was operated with plexiglass plates in place of the optics. Typical lasing gas mixtures were tried until uniform discharges at substantial specific power inputs were attained. With small changes in the percentage distribution of gases, the discharge continued to operate uniformly at high specific power input relatively independent of gas mixture. The two couplers were then employed to extract laser power at specific input powers of interest. During the 3-second output power measurements, it was necessary to cool the faces of the couplers with dry nitrogen to prevent possible thermal runaway. The gas mixture was experimentally optimized for the best combined electrical and mass flow efficiency and the following

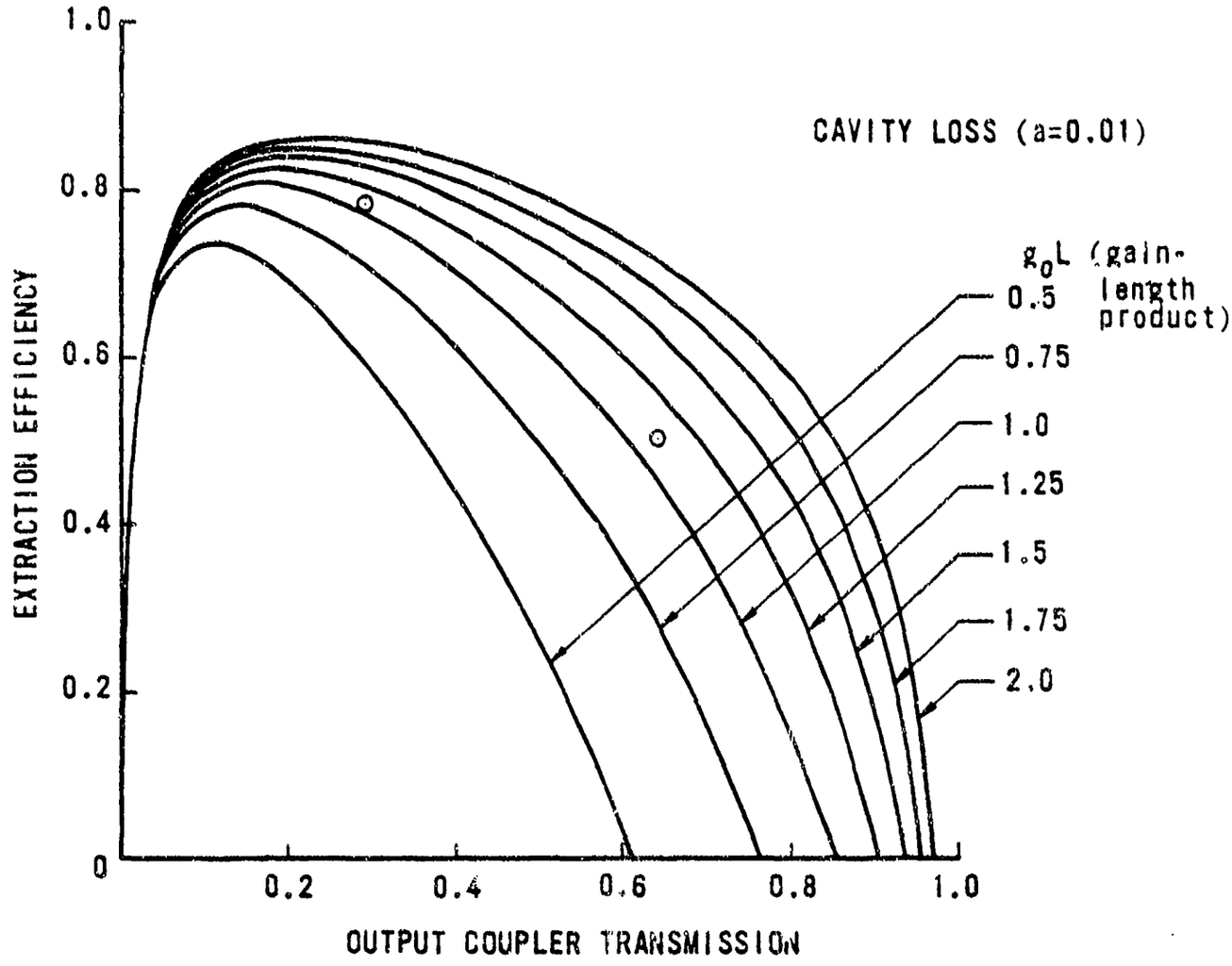

Figure 10. Extraction Efficiency Versus Output Coupler Transmission

measurements were recorded:

Active Cavity Length: Approximately 154 cm

Upstream Laser Pressure:

No Power Input: 30 Torr

With Power Input: 38 Torr

Mass Flowrate: CO_2 = 15.2 N_2 = 46.3 He = 29.6 mlb_m/sec

	Coupler 1	Coupler 2
Electrical Power Input:	31.8 kW	33.2 kW
Optical Power Input:	4725 Watts	6845 Watts
Specific Power Input to Discharge:	298 $kW/lb_m/sec$	290 $kW/lb_m/sec$
Total Efficiency:	14.8%	20.6%
Coupler Reflectivity:	0.36	0.71

The simultaneous solution of equation (23) for g_0L knowing the reflectivities of the optical components and the ratio of power outputs at constant specific power input under an estimated cavity loss of a = 0.01 yields $g_0L \approx 1.22$.

The corresponding extraction efficiences are indicated in figure 10 as circles for $g_0L \approx 1.22$ and t = 0.64 and 0.29. Note that if there were no transmission losses through the germanium coupler 2, this particular measurement would correspond to n_{tot} = 21.8 percent at a specific power output of 80 $kW/lb_m/sec$. The output beam measured 9.2 cm diameter which is greater than the geometrical spot size due to diffraction and transverse beam waist spreading of higher order modes. Assuming that the mirror is flood loaded inside the cavity, a simple geometrical cone would indicate that n_p is greater than 0.93. For $g_0L \approx 1.22$ and a lossless output coupler of t = 0.29, reference to figure 10 gives $n_{ext} \approx 0.79$. Recalling that

$$n_{elect} = n_{tot}/n_q n_m n_p n_{ext}$$

with

$$n_{tot} = 0.218$$

$$n_q = 0.41$$

$$n_m = 1.0$$

$$n_p = 0.93$$

$$n_{ext} = 0.79$$

gives $n_{elect} = 0.72$ which is less than a maximum value of 0.9 as reported in reference 5. With the active laser length fixed at L ≈ 154 cm, a low loss ZnSe output coupler with t = 0.25 was fabricated. The coupler transmission was chosen from figure 10 to be slightly higher than optimum for a = 0.01 in case cavity losses were greater than expected; this choice also places the coupler in a centrally located broad region of n_{ext}. With the assumption that the gas mixture can be adjusted to cause n_{elect} to approach 0.9, the best overall efficiency obtainable from the laser with L ≈ 154 cm is

$$n_{tot} = n_{elect}\, n_q n_m n_p n_{ext}$$

with

$$n_{elect} = 0.9$$

$$n_q = 0.41$$

$$n_m = 0.975$$

$$n_p = 0.93$$

$$n_{ext} \approx 0.80 \quad (a < 0.01,\ g_o L > 1.22)$$

$$n_{tot} = 0.27$$

A substantially longer laser cavity ($g_o L > 2$) with a long radius mirror ($n_p \rightarrow 1.0$) would give a maximum $n_{tot} \approx 0.31$). This potential 14 percent increase in n_{tot} was not considered pratical due to the increased operating voltages for the discharge and the difficulty in obtaining a uniform discharge at high specific power inputs for the longer length cavity. The current EDCL with L ≈ 154 cm operates at an $n_{tot} \approx 0.25$.

SECTION III

OPTIMIZED LASER PERFORMANCE

1. ELECTRICAL DISCHARGE

a. Electrode Placement

The present EDCL contains 16 electrodes which are sufficient to produce uniform discharges up to a combined current of 2.5 amps and a discharge voltage of 16 kilovolts per laser side.* This combination of current and voltage is in excess of that needed to heat the flowing gas to the temperatures required for optimum laser performance up to power output levels of 16 kilowatts.

The 16 electrodes were chosen after investigation of the total discharge current as a function of the number of anodes on a prototype of the present EDCL which used an array of 12 electrodes. The discharge was operated with symmetrical arrangements of 2, 3, 4, 6, and 12 anodes into a gas mixture near the optimum stated in section III.3. The current to the discharge was increased gradually until at some maximum current value the discharge arced. The discharge was not considered stable in these tests unless it operated without visible and electrical degradation for 5 seconds. This maximum current value was initially linear with increasing electrode numbers and then as the cathode glow increased to cover the cathode area, the current asymptotically approaced some constant for a much larger number of electrodes. For constant electrode number, the discharge arced at lower discharge currents for increasing cavity pressure. This was expected since electron recombination rates increase with increasing pressure and the increase in discharge voltage with pressure causes the electric forces along the discharge to overcome the aerodynamic forces used to stabilize it.

The effects of aerodynamic and electric forces were portrayed by several observations. First, a single anode discharge was observed to be forced toward the center of the cavity while radially diffusing in cross section as it moved toward the cathode. In fact, the discharge was forced across the cavity and terminated on the farthest away edge of the cathode. Second, two electrodes and higher number symmetrical arrangements caused the discharge

---

* The measurements reported in this section were obtained within the accuracies listed in the Appendix.

columns to be initially forced radially inward, but then these columns were observed to repel each other for increasing discharge voltages. Third, at a set discharge voltage, increasing the electrode number beyond some value did not appreciably increase the maximum current capability. This is apparently caused by ions from the closely spaced anodes merging and creating thermal instabilities. These last two effects were partially overcome in the electro-aerodynamic laser (ref. 5) by shocking the discharge in front of the anodes, hence, creating a more diffuse ion distribution. Fourth, the anodes were initially positioned close to the glass wall of the entrance section. The discharge was observed to operate in an annulus and the extracted laser energy had an absence of energy on the laser axis. The anodes were iteratively bent radially inward toward the laser axis until the discharge was uniform and no further increase in discharge current capability could be obtained. Thus, the aerodynamic forces between the anodes and the wall of the entrance section were adjusted for optimum performance in an experimental manner.

b. Electrical Characteristics of Discharge

The electrical discharge is characterized by a positive dynamic impedance and is plotted in figure 11 for various cavity pressures at the optimum gas mixture. This data was taken with laser power being extracted. The voltage across the discharge is approximately proportional with pressure and increases slightly with increasing current. The discharge is characterized by an average breakdown of E/P ≈4600 volts/cm-atm. The flatness of the voltage/current characteristic of the discharge indicates that the power supply ripple voltage (in the absence of a regulator) can cause appreciable variation in the discharge current and thus the laser power output.

In all cases the discharge progressed to an arc with increasing current above 2.5 amps characterized by several visible changes in the discharge. With increasing current the cathode glow gradually increased in area while visibly changing from a dull, uniform, violet color to separate regions of violet corresponding to each electrode. A further increase in current caused localized areas of intensely white light on the cathode (transition to abnormal glow region) followed by separation of the discharge near the cathode into a few individual columns. A slight increase in current above this region caused the discharge to arc which usually started from one or two anodes and rapidly progressed to several anodes. The two discharge columns for each side of the laser did not appear to interact.

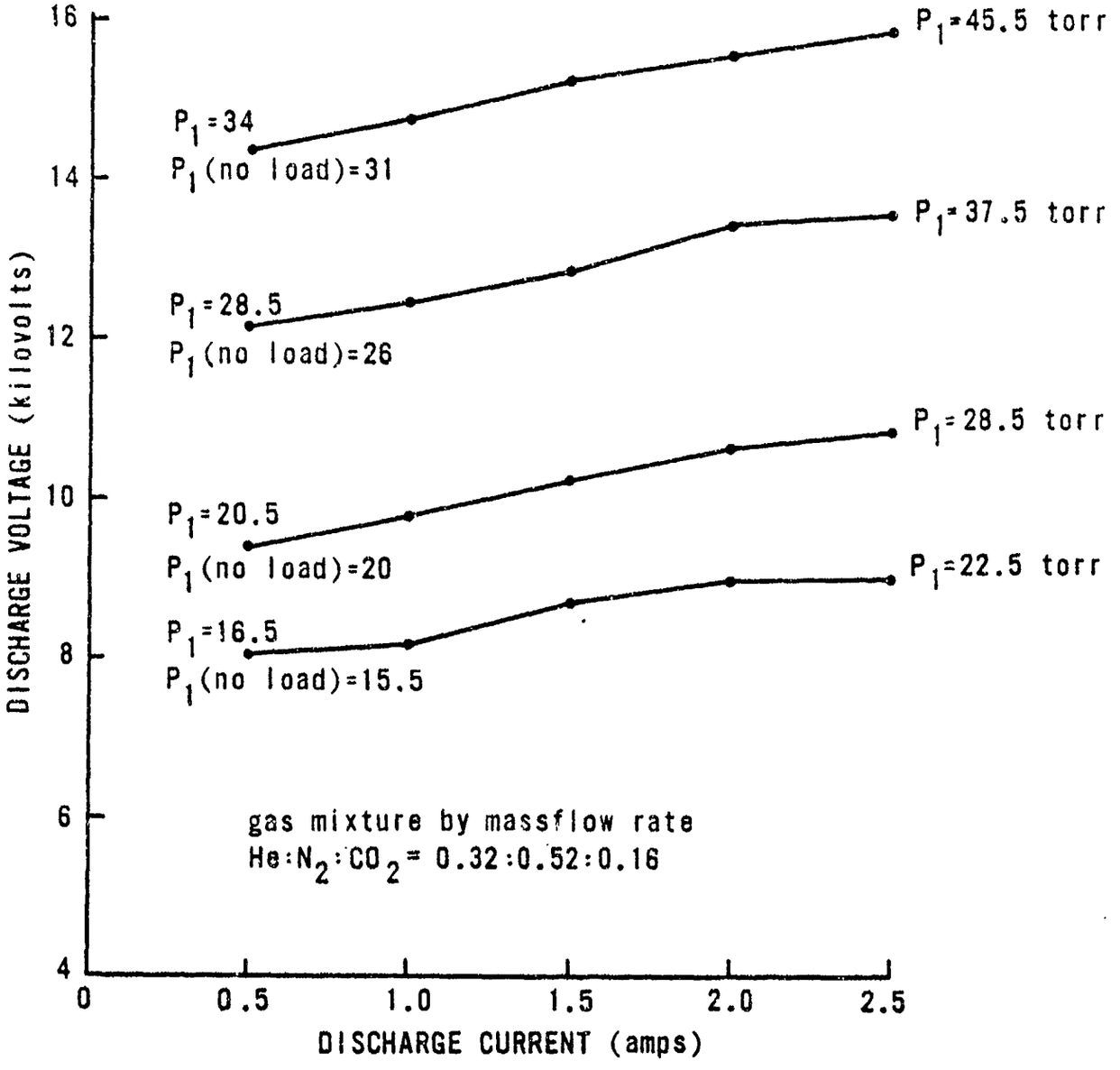

Figure 11. Discharge Voltage Versus Current

c. Effects of Flow on the Discharge

The annular exit to the laser channel was adjusted to provide a cold flow of 0.2 lb_m/sec at a cavity pressure of 40 torr for the optimum gas mixture flowrate ratio of $He:N_2:CO_2 = 0.32:0.52;0.16$. The entrance Mach number for this condition remained within 5 percent of $M_1 = 0.42$ over the pressure range of 15 to 40 torr. $M_1 = 0.42$ is higher than the calculated design value of $M_1 = 0.35$ stated in section II.3; however, the exit of the laser cavity acted in such a way that the exit pressure remained independent of specific power loading to the gas of up to 400 kW/lb_m/sec. The combined head loss at the laser exit due to the 90-degree annular exit, area ratios at the exit, frictional effects, and the opposing flows of the two laser halves acted as though the flow at the exit was "choked." Under these conditions the laser exit and 10-inch line back pressure remained constant during power loading. The entrance Mach number thus decreased with increasing specific power input below the design value of 0.35 for the highest specific input powers reported herein. The cold flow pressure drops throughout the laser were approximately 45 percent across the entrance electrodes, 10 percent along the laser cavity, and 20 to 25 percent across the laser exit giving a total pressure drop of 2.6 to 1. Since the exit pressure remained independent of the specific power loading, the pressure drop across the electrodes decreased with increasing specific power input due to the increase in entrance pressure. With aligned optics the cavity pressure ratio dropped by about 10 percent due to the reduction in gas temperature caused by the extraction of energy out of the cavity in the form of laser radiation.

Although only the laser cavity entrance pressure and temperature, and the exit pressure were measured; a reasonable prediction of entrance and exit Mach numbers and temperatures as a function of specific power input can be made. Recalling that the subscripts (1 and 2) refer to the entrance and exit parameters, respectively, solving equation (15) for $(M_2)^2$ gives

$$(M_2)^2 = \left[\frac{P_1}{P_2}(1 + \gamma M_1^2) - 1\right] 1/\gamma \qquad (28)$$

The Mach number (M) is related to the massflow rate ($\dot{m}$), pressure (P), temperature (T), gas constant (R), cross-sectional cavity area (A), and speed of sound (C) by

$$M = \frac{\dot{m}RT}{ACP} \tag{29}$$

If the Mach number given by equation (29) is at the cavity entrance, then the temperature (T), and hence (C), are independent of specific power input, and therefore,

$$P_1 = \frac{k}{M_1} \text{ and } P_2 \equiv \frac{k}{M_{10}} \tag{30}$$

where k is a constant M_{10} is the entrance Mach number with no power loading, and M_1 varies with specific power loading. Assuming a negligible pressure drop along the laser channel with no power loading, P_2 is independent of specific power loading in agreement with the experimental measurements of P_2. Substituting equation (30) into (28) gives

$$(M_2)^2 = \left[\frac{M_{10}}{M_1} (1 + \gamma M_1^2) - 1 \right] 1/\gamma \tag{31}$$

A similar substitution of equation (30) into (16) gives

$$\frac{T_2}{T_1} = \left(\frac{M_2}{M_{10}} \right)^2 \tag{32}$$

The specific power input ($P_g/\dot{m}$) is given by equation (18)

$$P_g/\dot{m} = C_p(T_{02} - T_{01}) \tag{33}$$

The entrance Mach number versus specific power input is plotted in figure 12. This plot is obtained by incrementing M_1 from $M_{10} = 0.44$ to $M_1 = 0.30$ in equation (31), using $(M_2)^2$ in equation (32), and solving for ($P_g/\dot{m}$) with equation (33). Figure 12 corresponds to a condition with $T_1 = 300°K$, $\gamma = 1.56$, $C_p = 1075$ j/lb$_m$°K, $P_1 = 26$ torr, and $\dot{m}$ per laser side of 0.068 lb$_m$/sec using the stated optimum gas mixture.

Pressure measurements were made while generating the voltage/current characteristics for figure 11. Figure 11 shows the entrance pressures measured under the conditions of 0, 0.5, and 2.5 amps for four cavity pressures from 15.5 torr to 31 torr. Plotted in figure 12 are the corresponding measured entrance Mach numbers for the conditions n = 0 (all electrical input power converted to gas heating) and n = 0.25 (75 percent of the electrical input power converted to gas heating, 25 percent to laser output power). The good agree-

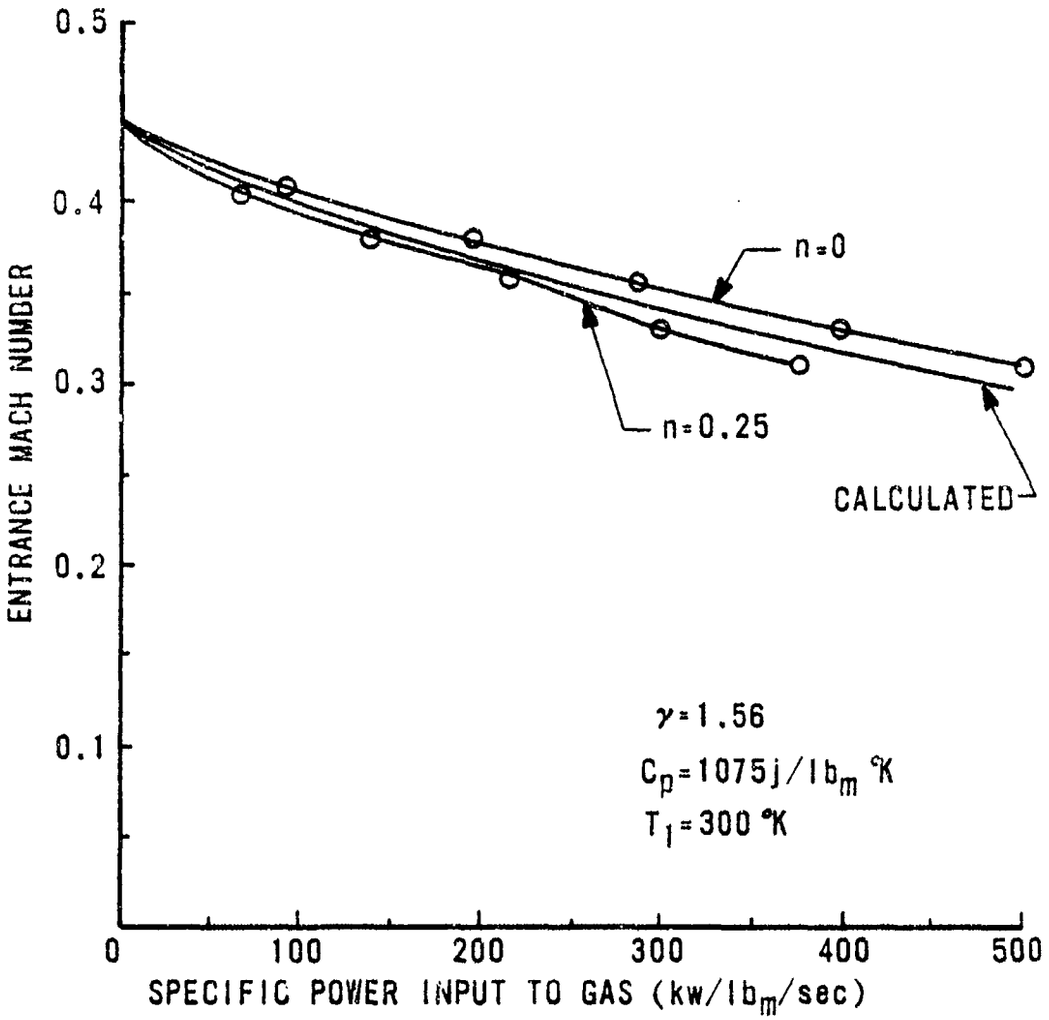

Figure 12. Entrance Mach Number Versus Specific Power Input to Gas

ment between the calculated entrance Mach number and the experimental Mach numbers for n = 0.25 confirms that the assumption made in section II.3 is valid. That assumption was that the extracted laser power represents a fractional loss of the total electrical power input to the laser channel.

Using equations (31) and (32), the exit Mach number and temperature are plotted in figure 13 for increasing specific power inputs. The highest output power of the laser was attained with a specific input power to the laser channel of 400 $kW/lb_m/sec$. The exit Mach number and temperature have an upper limit bounded by n = 0 and $P_g/\dot{m}$ = 400 $kW/lb_m/sec$ as shown on figure 13 and the upper limits on exit Mach number and temperature probably lie near the n = 0.25 region. The exit Mach number and temperature is expected to lie between $0.59 < M_2 < 0.63$ and $535°K < T_2 < 610°K$.

2. CURRENT REGULATOR

The effectiveness of the regulator was investigated under typical discharge conditions with optical laser extraction. Figures 14a, b, and c show the transient turn on characteristics of the power supply voltage, discharge current, and discharge voltage. These oscillograms were taken with the laser operating at a cavity pressure (cold) of 19 torr, discharge current per cavity side of 1.65 amps, discharge voltage of 9.8 kV, and a mass flow rate of 93 mlb_m/sec. Corresponding to these conditions the power supply voltage was 14.4 kV, resulting in a nominal voltage across the regulator of 2500 V and a laser output power of 8.1 kW.

The power supply voltage shown in figure 14a is up to normal operating voltage under 2 milliseconds with a ripple of 6.0 percent rms which is 2440 volts (p-p) for the stated voltage of 14.4 kV. Under certain power line conditions, it was observed that the power supply took two cycles to reach operating voltage although 80 percent of this value was always attained in less than 2 milliseconds. Figure 14b shows the transient suppression by the regulator of the first three cycles of power supply with the final operating current being attained in 10 milliseconds. The corresponding discharge current ripple is 6.3 percent rms or 0.59 amp (p-p) for the total current of 3.3 amps. The discharge voltage is shown in figure 14c as a series of positive spikes with a slight decay toward the next on cycle of the power supply. The initial turn on is characterized by an overvoltage to start the discharge followed by the 10-millisecond increase in voltage controlled by the regulator.

These measurements allow the actual operation of the regulator to be compared with that predicted by equation (14). Using values of $V_s = \pm 1220$ volts,

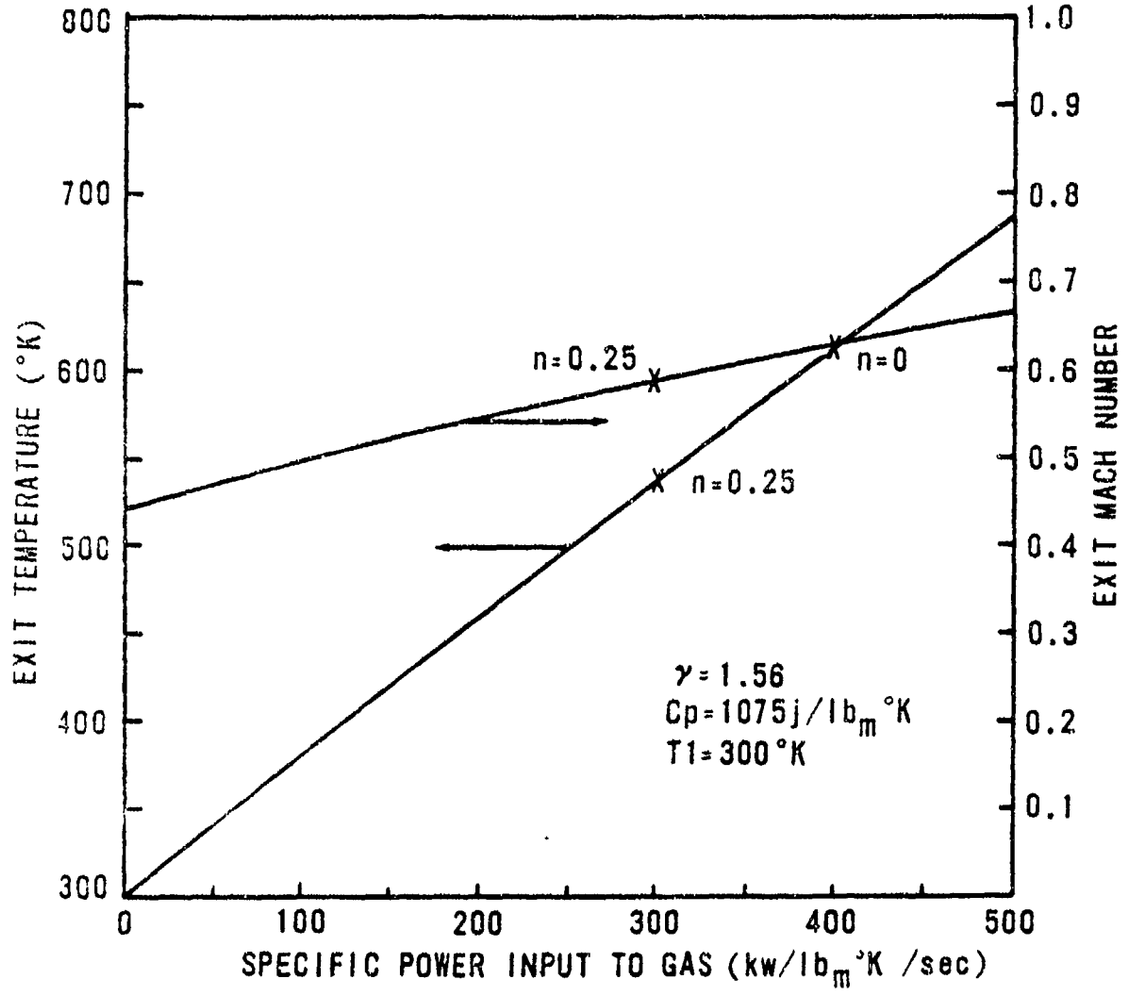

Figure 13. Exit Temperature and Mach Number Versus Specific Power Input to Gas

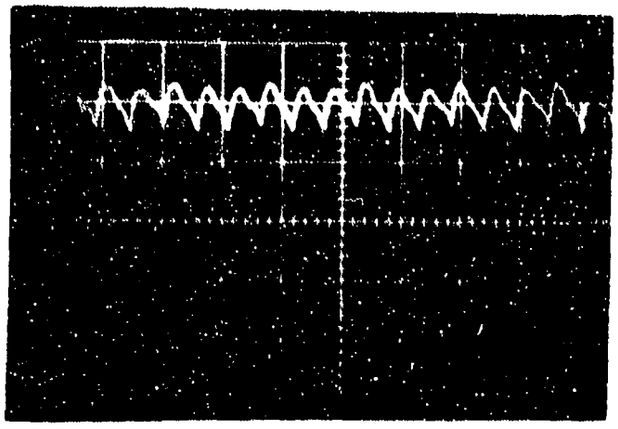

Power Supply Voltage
Vertical: 2.94 Kv/cm
Horizontal: 5 ms/cm

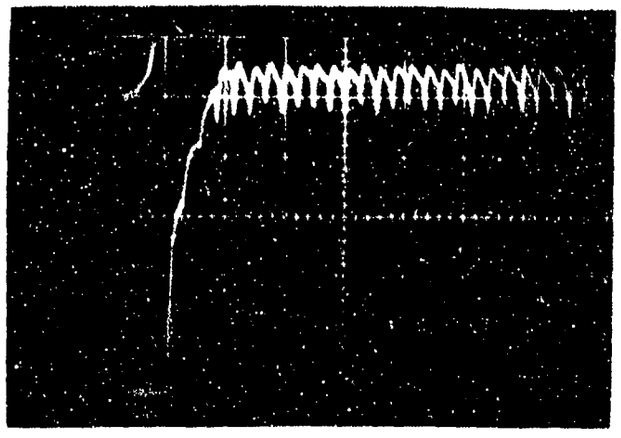

Discharge Current
Vertical: 0.65 amps/cm
Horizontal: 10 ms/cm

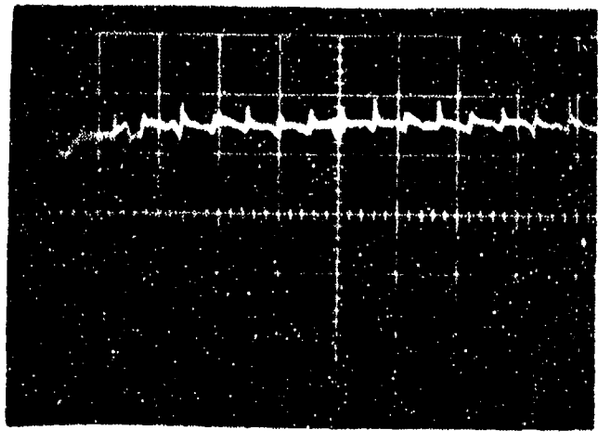

Discharge Voltage
Vertical: 2.18 Kv/cm
Horizontal: 5 ms/cm

Figure 14. Oscillograms of Electrical Discharge

V_{do} = 0, and r_d = + 700 ohms (from figure 11), equation (14) gives $i_t \approx \pm 0.081$ amp per laser side. The regulator performance is worse by a factor of (0.59)/(2)(0.081) (2) ≈ 1.8 than that predicted. This discrepancy in regulation and the positive voltage spikes of figure 14c are now discussed.

As the power supply voltage is increased to operate the laser at higher output power levels, the regulators lose their ability to control the discharge current against variations induced by the power supply ripple. The action of the regulator is to decrease its voltage for decreasing power supply voltage cycles in order to deliver constant current to the discharge load. At the suggested regulator operating condition of 2500 volts, it is possible for the plate-cathode voltage of the 8166 tubes to swing below the voltage required to maintain the 0A2 and 0B2 regulator tubes active. This results in the power supply ripple modulating the screen and grid voltages with a corresponding loss in module current regulation. Furthermore, the tube plate voltage approaches the region where the tube characteristics become nonlinear and the dynamic impedance contributed by the regulator approaches zero.

Measurements indicated that the module voltage must remain above 2000 volts in order that the screen voltage remain regulated, above 1400 volts for the grid voltage to remain regulated, and above 1000 volts to prevent the tube characteristics from becoming nonlinear. Hence, the desired operation of the power supply up to 20 kilovolts implies that the regulators should be operated near 3700 volts assuming a power supply ripple of 6 percent rms. This modification is not necessary since the primary purpose of the regulator is to keep the discharge current from increasing into an unstable region. This requirement is satisfied since the plate voltage always increases above the nominal 2500 volts for increasing changes in discharge current.

Referring back to figures 14b abd 14c, it is clear that the negative spikes in the discharge current and the positive spikes in the discharge voltage are caused by the regulator module voltage dropping from 2500 to 1280 volts on the negative cycles of the power supply ripple. Further tests were conducted by operating the modules at 3500 volts under the discharge conditions of this section. The discharge current ripple was 2.9 percent rms or 0.27 amps (p-p) for the total current of 3.3 amps. The regulator now performed ≈ 15 percent better than that predicted by equation (14).

This increase in predicted performance is probably due to the increase in μ of the tube with increased plate voltage.

Although the analysis of this section is based upon observing the change in discharge current induced by power supply variation, a review of equation (14) indicates that these measurements also give the change in current for an equal percentage change in discharge voltage with v_s set equal to zero. Equation (14) could be used to predict the effects of power supply variations coupled with discharge voltage changes on the output laser power due to perturbations in the cavity pressure and temperature. Neglecting the current ripple induced at the power supply frequency, the regulator maintained the discharge current within a few percent of nominal operating value both during and from run to run. The ripple of the power supply could be further reduced by using a standard filter section; however, this would increase the complexity of the laser system and increase the risetime of the output laser power.

3. POWER OUTPUT

Using a ZnSe output coupler coated in accordance with section II.5, the laser was operated over the cold flow cavity pressure range of 15 to 35 torr. The gas mixture was experimentally adjusted until the laser performed at a high combined electrical and mass flow efficiency. The optimum gas mixture by mass flow rate ratio was $He:N_2:CO_2 = 0.32:0.52;0.16$. This mixture resulted in uniform stable discharge performance at power outputs up to 15 kW at a specific power output of 100 $kW/lb_m/sec$ and a nominal electrical to optical efficiency of 25 percent. An efficiency slightly higher than 25 percent was acheived for a substantial increase in percent of both CO_2 and N_2. This increase in N_2 and CO_2 results in a gas mixture with significantly reduced specific heat and higher operating voltages. This more efficient mixture was not considered as optimum because of the decreased specific output power and instability of the discharge at the required higher operating voltages.

The laser operated reliability at a specific power output of 100 $kW/lb_m/sec$ up to a total output power of 15 kilowatts. The combination of higher discharge voltages and turn on transients of the power supply at higher output power levels resulted in either the primary circuit breakers tripping or the discharge separating into streamers with arcing. Both of these problems

could be circumvented by reducing the specific input power and selecting a more specialized (higher cost) power supply. The parameters for a 15-kW run are as follows:

Power Output - 15.4 kW

Discharge Current - 4.0 amps

Discharge Voltage - 15. 1 kilovolts

Mass Flow Rate - $He:N_2:CO_2$ = 48:78:24mlb_m/sec

Cavity Pressure - 30.0 torr (no load)
42.7 torr (with load)

Power Supply Voltage - 20.1 kilovolts

Specific Power to Gas - 300 $kW/lb_m/sec$

Specific Power Output - 103 $\pm$ 7.3 $kW/lb_m/sec$

Electrical to Optical Efficiency - 25.5 $\pm$ 1.3 percent

The total "wall plug" efficiency for the above data including losses in the power supply current regulator system, and the tube heater filaments is 17 percent.

At discharge voltages and currents approaching the above listed data (15 kilovolts and 4 amps), the discharge starts to separate into streamers near the cathode exit. Stable discharge performance for output powers of 15 kilowatts and above were obtained by lowering the discharge current and increasing the discharge voltage. The higher discharge voltage can be brought about by either increasing the total mass flow rate or the percentage of N_2. Either case results in the laser operating at a lower specific output power. The highest output power using this method was near 17 kilowatts.

The output power can be continuously adjusted over the range of 0.5 to 15 kilowatts by adjusting the discharge voltage, the discharge current, and the active gain length. The discharge voltage is adjusted over the range of 8 to 15 kilovolts by control of the mass flow rate and hence, the entrance cavity pressure (see figure 11). The six current regulators can be adjusted over the range of (0.25) 6 = 1.5 amps to (0.7) 6 = 4.2 amps. The gain length can be reduced by a factor of two by connecting the high voltage output of only three regulator tubes to one side of the laser. Reference to figure 10 and section II.5 would suggest that for two laser sides $g_0L \approx 1.22$ ($n_{ext} \approx 0.8$) and for one laser side $g_0L \approx 0.61$ ($n_{ext} \approx 0.7$). Since the extraction efficiency is nearly the same for one laser side as two laser sides combined, the output power for one side is slightly less

than one half of that attained with two sides. An additional reduction in output power is finally obtained by running one laser side with one regulator tube connected to all 16 ballast resistors over the range of current of 0.25 to 0.7 amp. The above techniques give a continuously variable range of 30 to 1 in output power. Although it was possible to lower the output power by decreasing the percentage of CO_2, the output beam quality did not remain uniform at the lower output power levels. The measured electrical to optical efficiencies under identical discharge conditions for one and two laser sides operating were $\eta_{tot} \approx 0.22$ and 0.26, respectively.

Measurements of the spatial characteristics of the output beam were determined with the aid of plexiglass burn impressions obtained in front of the output coupler (near field) and at various positions along the way to the focal plane (far field) of a mirror having a 2-meter radius of curvature. The beam profile was uniform and circular having a nearly ideal "top hat" profile with insignificant peak to trough modulation. Deviation from a uniform top hat profile only occurred in the vincinity of the focal plane of the mirror with a measured peak to trough modulation of about 5 to 10 percent. A scanning pyroelectric detector verified the above results.

The temporal history of the power output was recorded with a pyroelectric detector filtered for frequencies above kilohertz. The output beam was basically a replica of the time history of the discharge current. The temporal behavior of the output power was predominantly characterized by a 5 percent rms ripple at 360 hertz in agreement with the results of section III.2. Neglecting the effects of the ripple frequency, the output power fluctuated less than a few percent from the mean for runs up to 10 seconds in duration. The shot-to-shot variation in power output was also under a few percent although the optics had to be readjusted at times after 25 runs. The gradual accumulation of heat in the optical supporting structures (the glass laser cavity itself) caused a slight misalignment of the optics. Under these conditions, the beam profile differed slightly from circular and hence the output power was reduced by a small amount. The laser generally operated within 5 percent of a preset power for greater than 100 runs without the need for optical fine tuning.

The output beam divergence was measured by taking plexiglass burn impressions at 1, 2, and 3 meters from the output coupler giving a half-angle divergence of 3.3 milliradians. The effective diffraction number was

determined by measuring the minimum laser beam spot size in the focal planes of 0.5, 1, and 1.5 meter focal-length mirrors.

The diffraction number (N) may be defined as

$$N \equiv \left[\frac{(P_d/P_t)\ \text{theoretical}}{(P_d\ P_t)\ \text{experimental}} \right]^{1/2} \tag{34}$$

where (P_d/P_t) is the fraction of total power (P_t) from a gaussian beam that resides in the central Airy Disk of the diffraction limited, far-field beam pattern. For the case of the ideal diffraction limited gaussian beam, the theoretical value of (P_d/P_t) is $\simeq$ 0.86.

The total power (P_t) in the "top hat" beam profile of the EDCL at the focal plane of a mirror is the area (A) times the intensity (I) of the focussed spot. The power (P_d) is the intensity (I) times the area of the diffraction limited spot. The diameter (w) of the diffraction limited spot is related to the diameter (D) of the incident radiation at wave length (λ) on a mirror of focal length (f) by

$$w \simeq 2 \left(\frac{1.22\lambda f}{D} \right) \tag{35}$$

The experimental value of (P_d/P_t) is thus:

$$(P_d/P_t)_{\text{experimental}} = (\tfrac{\pi}{4} w^2) I/AI = \frac{\pi}{A} \left(\frac{1.22\lambda f}{D} \right)^2 \tag{36}$$

Using $\lambda \simeq 10^{-3}$ cm; f = 0.5, 1.0, 1.5 m; D = 10 cm; and the measured minimum spot areas for the three different focal length mirrors in equation (36), gives an average value of $(P_d/P_t) \simeq 2.3 \times 10^{-4}$. The effective diffraction number (N) given by equation (34) is

$$N \simeq \left[\frac{0.86}{2.3 \times 10^{-4}} \right]^{1/2} \simeq 60$$

The very large value of N is further evidence of the many high order transverse modes operating simultaneously in the high Fresnel number EDCL resonator. The above data also gives an algorithm which relates the focused spot size (d) to the mirror focal length (f) by

$$d \simeq 160 \left(\frac{\lambda f}{D}\right) \tag{37}$$

The total energy deliverable by the laser in a run is limited by the filling time of the gas reservoir and the thermal fracture limit of the ZnSe window. The maximum allowable thermal stress in the window is approximately given by

$$\sigma_{max} \simeq (\alpha Y)\overline{\Delta T} \tag{38}$$

where

$\sigma_{max} \simeq$ 6000 lb_f/in^2, maximum stress

$(\alpha Y) \simeq$ 70 lb_f/in^2 °K, product of thermal coefficient of expansion and Young's modulus

$\overline{\Delta T} \simeq$ average temperature rise in (°K) of the irradiated window area (assuming that the perimeter of the window remains at ambient temperature)

The average temperature rise of the window is approximately given by the one-dimensional, steady-state solution:

$$\overline{\Delta T} = \frac{(1 + 1/t)a_s + \beta_o \ell}{A\ell\rho C_p} E \tag{39}$$

where

t = transmission of window

a_s = surface coating absorption on window

β_o = bulk absorption of window material (cm^{-1})

ℓ = thickness of window material (cm)

A = area of laser beam through window (cm^2)

ρ = density of window material (gm/cm^3)

C_p = specific heat of window material (j/cm^3°K)

E = laser energy transmitted through the window (joules)

The values of the above constants for ZnSe used as a window on the EDCL are

$t \simeq 0.25$

$0.0015 < a_s < 0.002$

$0.001 < \beta_o < 0.005\,(cm^{-1})$

$\ell \simeq 0.95$ cm

$A \simeq 66\ cm^2$

$\rho C_p \simeq 1.9\ j/cm^3\ °K$

Using the values of absorption which will give the highest temperature rise, equation (39) gives

$$\overline{\Delta T} \simeq 1.2 \times 10^{-4}\ E \tag{40}$$

Statistically, ZnSe windows fracture at a stress of about 4000 lb_f/in^2. Substituting equation (40) into (38) gives a limit on the laser output energy of

$$E < \frac{4000}{(70)(1.2 \times 10^{-4})} \simeq 475 \text{ kilojoules}$$

As mentioned in section II.5, the ZnSe output coupler had a measured total attenuation of $\simeq 0.025$. The values of $a_s \simeq 0.002$ and $\beta o \simeq 0.005$ give a total attenuation of $\simeq 0.01$. It is assumed that the discrepancy between the measured and predicted attenuation is due to the difficulty in measuring the coating losses on a two-sided window where there can be appreciable scatter from the surfaces and throughout the bulk material. If we assume the attenuation of 0.025 is due to poor coatings, then the values of the surface and bulk absorption could be as high as $a_s \simeq 0.01$ and $\beta o \simeq 0.005$. These absorption values substituted in equation (39) give an energy limit of $E < 125$ kilojoules.

The above predictions of the transmitted energy limit neglected the loss of absorbed window energy which occurs due to radial conduction and surface convection. The energy limit as calculated is pessimistic.

The EDCL has been operating with the same ZnSe window for greater than 2400 minutes of lasing time. This corresponds to 28,000 runs of 5 seconds each at an average power output of 10 kilowatts giving a total transmitted energy in excess of 1.4 gigajoules. During this period of operation, an energy limit of 100 kilojoules was employed and no appreciable heating of the output coupler ever occured. The completed AFWL EDCL is shown in figure 15.

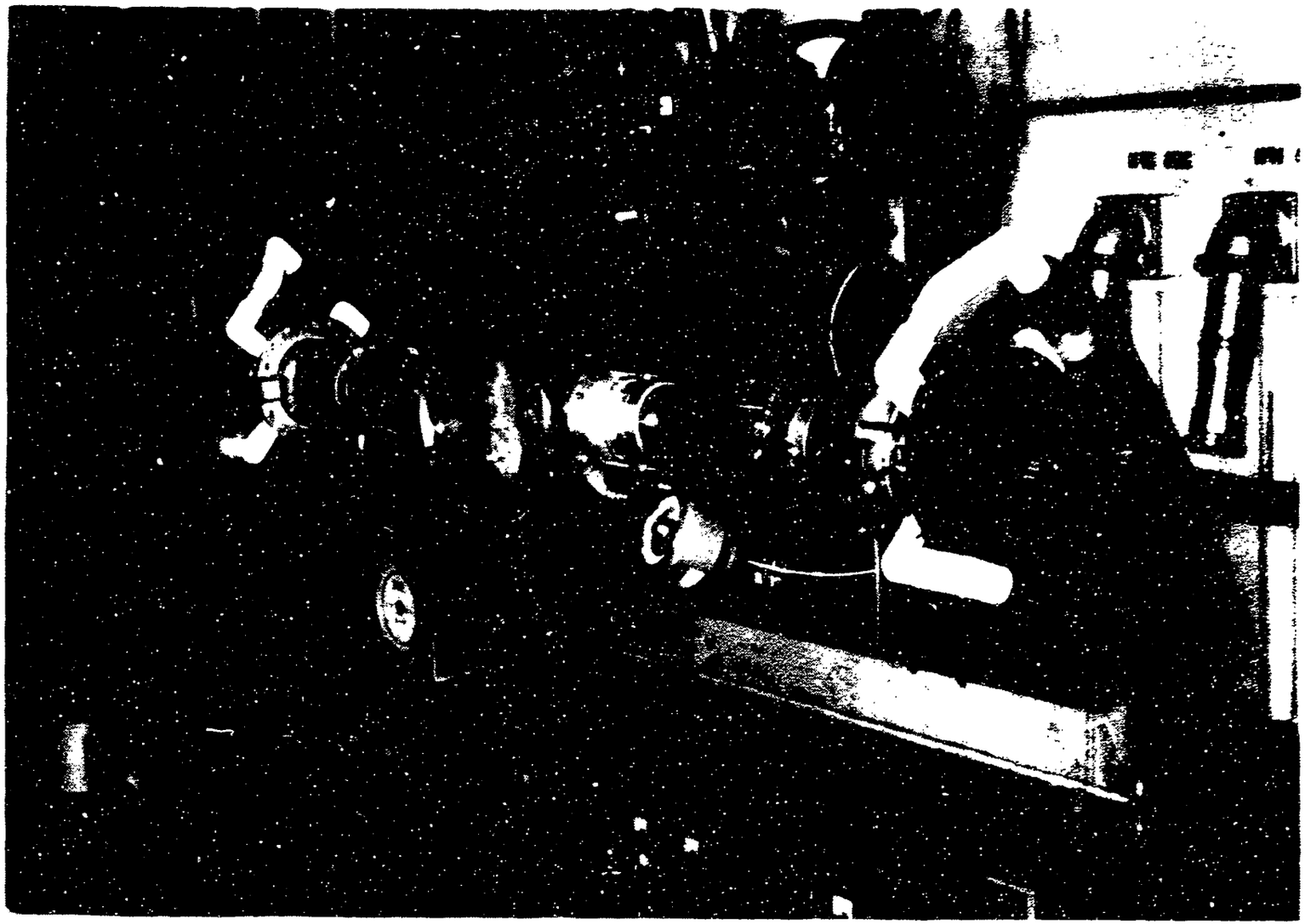

Figure 15. AFWL Electric Discharge Coaxial Laser System

SECTION IV

CONCLUSIONS

A high output power laser device offering simplicity of construction, low cost, high reliability, and "push button"-type operation has been built and demonstrated. The EDCL system extracts power in excess of 15 kilowatts routinely at a nominal electrical efficiency of 25 percent and a mass flow efficiency of 100 $kW/lb_m/sec$. The output beam intensity is circular, uniform, temporally stable, and repeatable within 5 percent.

The technique of introducing controlled aerodynamic forces on the gas entering a laser cavity can be used to produce and stabilize large volume, high power gas discharges. The success of operating the EDCL at the maximum output power is based upon the availability of ZnSe material in large sizes that can be appropriately coated to serve as both an output window and reflective component of an optical resonator.

REFERENCES

1. Hansen, Arthur G., Fluid Mechanics, Wiley, pp 223-283, 1967.

2. Hill, Alan E., "Role of Thermal Effects and Fast Flow Power Scaling Techniques in CO_2-N_2-He Lasers," Appl. Phys. Ltrs., Vol. 16, pp 423-426, June 1970.

3. Hill, Alan E., "Continuous Uniform Excitation of Medium-Pressure CO_2 Laser Plasmas by Means of Controlled Avalanche Ionization," Appl. Phys. Ltrs., Vol. 22, p 670-673, June 1973 (and extension of this work presently being conducted at the Air Force Weapons Laboratory, KAFB, NMex).

4. Hill, Alan E., "Uniform Electrical Excitation of Large-Volume High-Pressure Near-Sonic CO_2-N_2-He Flowstream," Appl. Phys. Ltrs., Vol. 18, p 194-197, March 1971.

5. Hill, Alan E., Hamil, Roy A. et al., "Electro-Aerodynamic Laser Technology," Laser Division Digest, LRD-71-2, Air Force Weapons Laboratory, Kirtland AFB, NMex, Fall 1971.

6. Fox, A. G., Li, Tingye, "Resonant Modes in a Laser Interferometer," Bell Sys. Tech. J., Vol. 40, pp 453-488, March 1961.

7. Kogelnik, H., Li, Tingye, "Laser Beams and Resonators," Proc. IEEE, Appl. Opt., Vol. 54, pp 1312-1329, Oct. 1966

8. Rigrod, W. W., "Saturation Effects in High-Gain Lasers," J. Appl. Phys., Vol. 36, pp 2487-2490, August 1965.

9. Davis, J. W. et al., Investigation of a High Power Electric Discharge Laser, UARL Report H-910676-10, United Aircraft Research Laboratories, East Hartford, CT, 26 November 1969.

APPENDIX

MEASUREMENT STANDARDS

The measurements reported are based upon the following calibrated standards and were recorded within the indicated accuracy:

Current and Voltage (1%) - Fluke Model 8100A digital multimeter

Static Cavity Pressure (2%) - Wallace and Tiernan Model FA160 absolute gage

Mass Flow Rate (5%) - Standard sharp-edged sonic orifices with upstream pressures referenced against a Heise absolute pressure gage

Temperature (5%) - Standard chromel-alumel junction with indicated output on a Keithley Model 155 Null Detector Microvoltmeter

Optical Power Output (5%) - Coherent Radiation Model 213 power meter referenced against a RDF Corp. (Hudson, N.H.) Model 28900 hollow-copper cone calorimeter (This device can be electrically calibrated via an internal heat source to within 1 percent).